White Rose Research Online

eprints@whiterose.ac.uk
https://eprints.whiterose.ac.uk
Universities of Leeds, Sheffield and York

Deposited via The University of Leeds.

White Rose Research Online URL for this paper:
https://eprints.whiterose.ac.uk/id/eprint/239304/

Version: Accepted Version

Article:
Xu, L., Lin, T., O'Hern, S. et al. (2026) When feeling safe becomes risky: A VR-EEG-computer vision framework for analyzing cyclist safety in dynamic traffic environment. Accident Analysis & Prevention, 229. 108418. ISSN: 0001-4575

https://doi.org/10.1016/j.aap.2026.108418

This is an author produced version of an article published in Accident Analysis & Prevention, made available via the University of Leeds Research Outputs Policy under the terms of the Creative Commons Attribution License (CC-BY), which permits unrestricted use, distribution and reproduction in any medium, provided the original work is properly cited.

Reuse
This article is distributed under the terms of the Creative Commons Attribution (CC BY) licence. This licence allows you to distribute, remix, tweak, and build upon the work, even commercially, as long as you credit the authors for the original work. More information and the full terms of the licence here: https://creativecommons.org/licenses/

Takedown
If you consider content in White Rose Research Online to be in breach of UK law, please notify us by emailing eprints@whiterose.ac.uk including the URL of the record and the reason for the withdrawal request.

UNIVERSITY OF LEEDS
University of Sheffield
UNIVERSITY of York

When Feeling Safe Becomes Risky：A VR-EEG-Computer Vision Framework for Analyzing Cyclist Safety in Dynamic Traffic Environment

Lurong Xu[1], Tengfeng Lin[2], Steve O'Hern[3], Alexa Delbosc[1], Zhuo Chen[1], Inhi Kim[2], Shuli Luo[4]

1. Department of Civil and Environmental Engineering, Monash University, Clayton VIC 3800, Australia
2. Cho Chun Shik Graduate School of Mobility, Korea Advanced Institute of Science and Technology, Daejeon, South Korea
3. Institute for Transport Studies, University of Leeds, Leeds LS2 9JT, UK
4. School of Humanities and Social Science, The Chinese University of Hong Kong, Shenzhen, China

Corresponding author: Shuli Luo; The Chinese University of Hong Kong, Shenzhen, Guangdong, China; Email: shuliluo@cuhk.edu.cn

Abstract

The mismatch between cyclists' perceived safety and actual crash risk in mixed-traffic environments is a critical yet underexplored issue in road safety research. While prior studies have focused on static environmental factors, they often overlook the real-time influence of dynamic visual stimuli on risk perception. To address this gap, this study developed a multisource-integrated virtual reality (VR) experimental platform that synchronously captured millisecond-level electroencephalography (EEG) signals from 72 participants, built environment (BE) features, and time-to-collision (TTC) data from VISSIM microsimulation. A Long Short-Term Memory (LSTM) model was used to examine how mismatches emerge between perceived safety and crash risk. Results reveal a 'perceptual relief period' after being overtaken, where cyclists exhibit higher perceived safety despite persistent threats from following vehicles, creating a potentially hazardous temporal window. This mismatch effect is further amplified in environments characterized by high spatial enclosure, complex visual textures, dense vegetation, and low visible vehicle density. These findings suggest that BE features intended to enhance aesthetic appeal or reduce stress may inadvertently impair cyclists' ability to perceive risk in high-conflict areas. This study offers empirical support for an integrated human–vehicle–environment safety framework and calls for interdisciplinary collaboration between neuroscience and transport engineering in the design of safer mobility systems.

Keywords: cyclist safety, Virtual Reality, computer vision, bike simulator, electroencephalography

1. Introduction

Cycling safety has become a pivotal concern for sustainable urban development, particularly in mixed-traffic environments where cyclists share roadways with motor vehicles (Rasch and Dozza 2020, Rasch *et al.* 2022). The complex interaction between cyclists and vehicles significantly elevates the potential risks of a crash (Terum and Svartdal 2019). As vulnerable road users, cyclists face higher risks of severe injury or fatality in crashes (Bogacz *et al.* 2021). However, cyclists are often exposed to mixed-traffic conditions in areas such as historic districts or residential roads, where heritage or physical constraints limit the feasibility of cycling infrastructure (Pucher and Buehler 2008, Xu *et al.* 2025). This continued exposure to high-risk environments may lead cyclists to adapt or become desensitized to traffic hazards, resulting in a mismatch between perceived safety and actual risk (Bazilinskyy *et al.* 2020).

Existing research shows a clear split between objective and subjective understandings of cycling safety. On one hand, considerable progress has been made in objective risk quantification through conflict and crash analysis (Bazilinskyy *et al.* 2020, Bogacz *et al.* 2021). On the other hand, growing attention has been paid to perceived safety, which plays a key role in shaping cycling behavior and has shown strong explanatory power for cycling frequency (Aldred 2016, Olsson and Elldér 2023). Notably, as spatial visual information is a primary input to the human perceptual system, street-level built environment (BE) features (e.g., greenery) are closely linked to how safe a space feels (Ito and Biljecki 2021). However, empirical evidence reveals a paradoxical phenomenon: road sections perceived as "safe" by cyclists frequently coincide with locations

exhibiting elevated traffic conflict rates (Ye *et al.* 2024). The main explanations are objective assessment mainly focusing on the vehicle-human interactions, whereas perceived safety is more sensitive to visual environmental features encountered along cycling routes (Ito and Biljecki 2021, Olsson and Elldér 2023). Current approaches thus fail to capture how dynamic BE conditions influence real-time risk perception, limiting insights into the spatiotemporal variability of subjective safety assessments and their implications for accident prevention (Bogacz *et al.* 2021).

This research gap is compounded by two methodological limitations. First, traditional approaches struggle to quantify the dynamic nature of surrounding visual elements. Static tools, such as street-view imagery or audit records, capture BE features as fixed snapshots, failing to reflect the dynamic visual information that cyclists actually experience, such as passing vehicles (Nazemi *et al.* 2021). In reality, cyclists' safety perception is a neurocognitive process continually updated, corresponding to dynamic environments (Bidgoli *et al.* 2025). These dynamic features not only affect momentary exposure to potential risk but also shape perception through attentional processing (Galpin *et al.* 2009). Second, the temporal resolution of subjective safety measurement remains limited. Retrospective questionnaires, commonly used in prior studies, lack the granularity to trace how safety perceptions evolve millisecond-to-millisecond, inevitably missing transient yet decisive cognitive shifts (Bogacz *et al.* 2021).

To address these limitations, this study aims to investigate the mismatch between objective and subjective cycling safety in mixed-traffic environments. By designing an integrated experimental system combining virtual reality (VR) cycling simulation, electroencephalography (EEG), VISSIM

traffic microsimulation, and employing Long Short-Term Memory (LSTM) modeling, this research aims to answer two core questions: 1) How do mismatches between cyclists' perceived safety and actual crash risks emerge in mixed-traffic environments? and 2) how do BE features modulate these mismatches? This study contributes to overcoming technical limitations in existing research by capturing the dynamic interplay between BE and perception in real time. In addition, it identifies key BE features associated with the emergence of perception–risk mismatches, offering actionable insights for policy implications in shared traffic spaces.

2. Literature Review

2.1. Cyclists' perceived safety and influential factors

Perceived safety is typically conceptualized as a psychological state involving individuals' cognition of potential risks and subsequent transportation choices (Cho *et al.* 2009). Research has consistently identified vehicle-cyclist interactions as primary determinants of perceived safety, with maneuvers such as overtaking or close following particularly influencing cyclists' risk assessments (Aldred 2016). Demographic features also moderate these risk perceptions; for instance, female and older adults often exhibit heightened sensitivity to high-potential-risk events, particularly in response to close-passing incidents (Griffin *et al.* 2020). However, perceived safety is shaped not only by interactions among road users but also by the sensory processing of visual information critical to risk identification (Bogacz *et al.* 2021). Recently, it has been demonstrated that cyclists' visual scanning behavior extends beyond the central roadway area, with peripheral vision playing a broader and more dynamic role in identifying environmental cues (Galpin *et al.* 2009). This

expanded visual field underscores the importance of street-level built environment (BE) features, which shape cyclists' perceptions of safety through both direct visual information channels and more subtle environmental psychology mechanisms (Xu *et al.* 2025). Greenery, for instance, positively affects cyclists' perceived safety by eliciting favorable emotional reactions and lowering psychological stress, thus facilitating risk evaluation and decision-making (Ye *et al.* 2024). Similarly, visual complexity characterized by visual elements such as color diversity, textural variation, and visual entropy, influences perceived safety by modulating cognitive load, attention distribution, and the efficiency of hazard recognition (Lynch 1964, Kawshalya *et al.* 2022, Xu *et al.* 2026).

Despite growing recognition of these relationships, current methodological approaches to evaluating perceived safety exhibit certain limitations. Many studies rely on static images or post-ride questionnaires, which fail to capture the dynamic nature of cyclists' moment-to-moment psychological responses (Manton *et al.* 2016, Ito and Biljecki 2021). These methods inadequately represent essential stimuli, such as fluctuating vehicle speeds, ambient noise, or the lateral distance of passing traffic, which are vital to the real-time perception of risk (Nazemi *et al.* 2021). Moreover, the use of static images can induce bias in visual scanning patterns for risk cues, as participants may rely on prior knowledge rather than actively responding to immediate risks (Galpin *et al.* 2009). In contrast, real-world cycling perception is shaped by continuous sensory input and requires moment-to-moment adaptation to rapidly changing conditions (Bogacz *et al.* 2021). This distinction is supported by physiological evidence: for instance, studies show that cyclists' heart rates rise significantly during overtaking events, clearly indicating that perceived safety fluctuates in response to transient environmental changes (Doorley *et al.* 2015). Additionally, retrospective methods are

prone to recall bias and passive evaluation, as participants do not experience the scenarios from an embodied first-person perspective (Bogacz *et al.* 2021). These limitations highlight the need for methodological approaches that can capture cyclists' safety perceptions with higher temporal resolution and ecological validity.

2.2. Discrepancies between actual risk and perceived safety

Traditional cycling safety research frequently employs Surrogate Safety Measures (SSMs), such as Time-to-Collision (TTC), to objectively quantify potential crash risk between two road users (Campisi *et al.* 2020). TTC refers to the estimated time remaining before two road users would collide if they continued on their current trajectories at constant speeds (Campisi *et al.* 2020). When TTC falls below a certain threshold, there exists a risk of potential collision (Ge *et al.* 2019). In scenarios involving interactions between cyclists and motor vehicles, this TTC threshold is generally set between 2 and 3 seconds (Darzian Rostami *et al.* 2020, Rasch *et al.* 2020). However, these studies primarily focus on observable external interactions and often neglect the internal cognitive processes of cyclists that mediate cyclists' risk perception and response behaviors (Cho *et al.* 2009).

In real-world traffic conditions, people's perception of risk in traffic interactions frequently occurs later than what is reflected by SSMs (Zhao *et al.* 2021). This delay might result from a lag in awareness of imminent danger. For example, a driving vision experiment demonstrated that drivers typically required more than 450 milliseconds to notice hazards from emerging vehicles (Galpin *et al.* 2009). Additionally, cyclists often postpone braking until they explicitly perceive the

threat, even when TTC values have already fallen below critical thresholds (Johnson *et al.* 2010). Therefore, while SSMs are effective in objectively identifying high-risk situations, they may fail to capture cyclists' real-time response, potentially creating systematic discrepancies between perceived safety and actual risk exposure.

These discrepancies become more pronounced when considering built environment influences. For instance, residential streets with abundant greenery may be perceived as safe but are sometimes associated with higher crash rates due to increased visual complexity (Ye *et al.* 2024). Kononov *et al.* (2007) emphasized the importance of aligning perceived and actual safety. When actual risk is high but perceived risk is low, it may suggest that BE features obscure potential hazards (Schneider *et al.* 2004). Conversely, a high perceived risk despite low actual risk may reflect environmental ambiguity, calling for proactive measures (Cho *et al.* 2009). Explanations such as risk homeostasis propose that individuals reduce caution in seemingly safer settings (Wilde 1998, He *et al.* 2021). Additionally, excessive visual complexity may impair hazard recognition and lead to misjudged safety (Cho *et al.* 2009, Ye *et al.* 2024). Although these hypotheses offer plausible interpretations, empirical validation remains limited. Understanding the mechanisms behind such mismatches is essential for improving risk assessment and safety interventions.

2.3. Advances in fused data collection methods

Recent advancements in multimodal data fusion offer opportunities to address the limitations described above. EEG effectively measures cognitive states, attentional processes, and perceived risks in transportation research (Ma *et al.* 2024, Yang *et al.* 2025). Within the EEG spectrum, the α

band (8–13 Hz) serves as a critical neural marker for perceived safety, as its oscillations modulate cortical excitability and attentional allocation (Palva and Palva 2007, Yeom *et al.* 2021). Specifically, a decrease in α power typically signals heightened vigilance to external stimuli, whereas an increase reflects internalized attention and a relaxed, non-threatening state (Roth and Cohen 1986, Choi *et al.* 2015, Chatterjee *et al.* 2023). The validity has been further verified in cycling-specific environments. For example, Bogacz *et al.* (2021) established α power as a reliable indicator of cyclists' risk perception, demonstrating that its reduction correlates with both heightened instantaneous risk and an increased likelihood of braking. Similarly, Bidgoli *et al.* (2025) found that α wave shows the strongest association with self-reported safety ratings, where higher perceived safety consistently corresponds to elevated α power, which underscores the central role of the α band in the neurophysiological assessment of cycling safety.

Virtual Reality (VR) technology further addresses limitations inherent in static assessments by realistically simulating dynamic environments (Nazemi *et al.* 2021). Compared to static image assessments, VR significantly improves ecological validity and measurement accuracy by enabling controlled and repeated exposure to dynamic risks (Bogacz *et al.* 2021). Extensive studies confirm that VR experiences accurately reflect participants' subjective safety perceptions due to realistic responses elicited in dynamically changing scenarios (Dang *et al.* 2024, Kwon *et al.* 2024). Integrating VR with EEG offers novel insights into cognitive responses during real-time risk scenarios (Bogacz *et al.* 2021). Magosso *et al.* (2019) have demonstrated in a VR experiment that tasks requiring increased attentional demand led to a decrease in α-wave power, while less demanding scenarios result in increased α-wave power, highlighting the combined methods' utility

for understanding dynamic safety perceptions.

In addition, advancements in computer vision (CV) technology further enable precise quantification of BE features. Extensive studies employing semantic segmentation techniques on large-scale street-view image datasets have successfully extracted pixel-level BE features, including greenery, building, and vehicle densities (Ito and Biljecki 2021, He and He 2023, Xu *et al.* 2025, Luo *et al.* 2026). The use of CV to extract BE features within VR environments has further illustrated the value of integrating these technologies, as it supports the development of a robust framework that links objective environmental conditions with real-time fluctuations in perceived safety (Luo *et al.* 2025).

However, a significant research gap remains: although VR, EEG, and CV technologies have been individually applied in cycling safety research, few studies have systematically integrated these tools to investigate the mechanisms underlying the discrepancies between perceived and actual safety in cycling environments.

3. Method

Figure 1 outlines the methodological framework of this study. A controlled experiment involving 72 participants enabled synchronous high-resolution data collection across three dimensions: (1) dynamic extraction of BE features from cyclists' first-person perspectives using computer vision technology; (2) continuous EEG recordings reflecting neural correlates of subjective safety; and (3) TTC metrics derived from simulations to quantify actual crash risk.

To support this integration, a VR environment, a bike simulator, and the traffic microsimulation tool VISSIM 2023 were all integrated within the Unity 3D platform. Participants experienced immersive VR cycling scenarios while their first-person views were recorded through the VR headset. These recordings were segmented into frames at 100-millisecond intervals to ensure a unified temporal reference across all data sources. Computer vision techniques were applied to extract BE features from each frame, and these were timestamped accordingly. Simultaneously, trajectory data and raw EEG signals were synchronized to the same temporal resolution and preprocessed for quality assurance. Real-time TTC values were calculated to represent actual risk, while relative alpha power extracted from EEG signals served as an indicator of perceived safety. Based on the temporally aligned dataset, an LSTM model was constructed to examine how mismatches arise between perceived and actual risk. The model's interpretability provided insights into the underlying mechanisms contributing to such discrepancies.

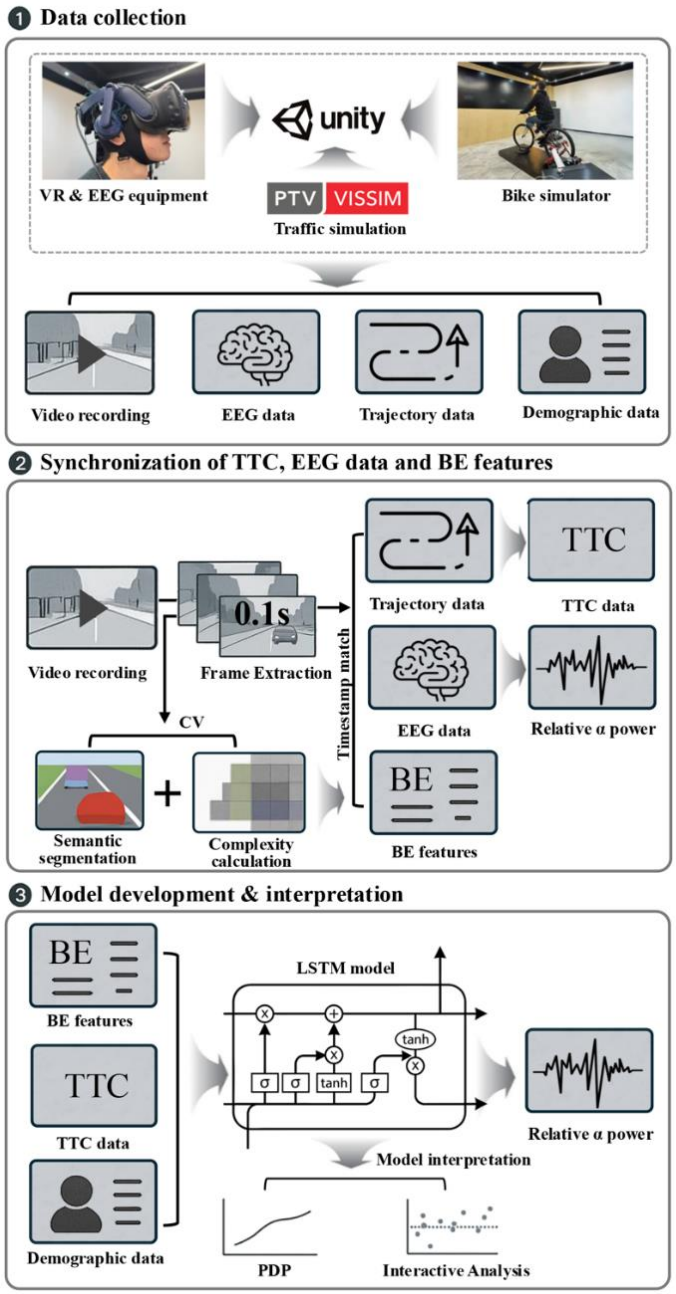

Figure 1 Methodological framework

3.1. Scenario setting

The scenario setting for this study was based on a 2×3 factorial experimental design, incorporating two traffic volume conditions (1,500 vehicles/hour and 500 vehicles/hour) and three greenery coverage levels (high, medium, low), drawn from the characteristics of urban streets in the

historic city area of Suzhou, China. The experimental road segment was set at a total length of 650 meters, featuring an 8-meter-wide two-way single-lane cross-section (4 meters per direction). This geometric layout reflects typical street forms in Suzhou's historic city, where heritage preservation restricts 75.1% of mixed-traffic roads to an average width of 8 meters (Xu *et al.* 2025). Given that the minimum legal width for a cycle lane is 2.5 meters, implementing physically separated bike lanes is impractical (Suzhou Planning Bureau 2022), making mixed-traffic conditions a realistic and policy-constrained baseline for studying inherent conflicts.

Greenery (Figure 2) was manipulated by varying the tree canopy coverage along the street (Zhu *et al.* 2022), with three levels established: 10% (low), 50% (medium), and 90% (high). The highest level, 90%, is often used to represent "tree-lined" boulevards in mixed traffic areas, intended to enhance environmental quality and influence people's perceptions of safety and comfort (Sarkar *et al.* 2015). To ensure a range of environmental conditions, additional settings at 10% and 50% canopy coverage were included. The buildings on both sides of the simulated street were modeled after the local architectural style of Suzhou's ancient city, with certain differences introduced into the facades to reflect real-world variability.

Traffic volume settings were guided by the Traffic Level of Stress (TLS) framework, which categorizes cyclists' perceived safety under varying traffic conditions (Mekuria *et al.* 2012). In accordance with the Chinese Road Traffic Safety Law Implementation Regulations, the maximum allowable speed on urban roads was capped at 50 km/h (The State Council of the People's Republic of China 2019). Based on this constraint, two traffic volume conditions were defined for mixed

traffic environments: Level 2 (500 vehicles/hour) and Level 3 (1500 vehicles/hour), consistent with TLS adaptations for such scenarios. Traffic flow patterns were simulated using VISSIM, and the Wiedemann 99 (W99) car-following model was employed to realistically capture bicycle–vehicle interactions. W99 is designed to reflect both psychological thresholds and physical constraints during key driving maneuvers such as free driving, closing in, following, overtaking, braking, and emergency stopping, and it has been widely applied and validated in previous studies focusing on bicycle–vehicle conflict scenarios (Wiedemann and Reiter 1992, Xu *et al.* 2023).

Figure 2 Variable setting of greenery

3.2. Data collection

3.2.1. Apparatus

An integrated experimental platform was developed using Unity 3D as the central framework for coordinating multimodal data collection and reproducing mixed-traffic environments with high

fidelity. The core of the experimental setup was a fixed-base bicycle simulator, consisting of a stationary bicycle mounted on a static platform equipped with a steerable handlebar, a rear-wheel speed encoder, and a brake force sensor (Figure 3a). Participant actions—steering, pedaling, and braking—were converted into electrical signals, processed in Unity via rigid-body dynamics to compute real-time bicycle displacement, velocity, and heading within a closed-loop control system.

Visual output was delivered through an HTC VIVE Pro 2 headset (Figure 3a), offering 4896 × 2448 resolution, 120 Hz refresh rate, and sub-millimeter spatial tracking (HTC Corporation 2025). Static elements such as buildings and greenery were 3D modeled and rendered in Unity, while dynamic traffic flows were generated by VISSIM. A custom C# COM interface enabled real-time bidirectional communication, projecting VISSIM-generated vehicle trajectories onto the Unity coordinate system (Ramadhan *et al.* 2019, Xu *et al.* 2023). In parallel, participants' cycling behaviors such as steering, pedaling, and braking were captured by the bike simulator and transmitted to VISSIM via Unity 3D, allowing motor vehicle movements to be dynamically influenced by the cyclist's real-time responses. All trajectories were recorded at 60 frames per second for precise spatiotemporal analysis.

Concurrently, EEG signals were recorded using a 32-channel EMOTIV EPOC Flex wireless system (Figure 3b-c), fitted with a flexible saline electrode cap arranged according to the international 10–20 system, with the CMS and DRL electrodes serving as references (Yang *et al.* 2025). Data were sampled at 256 Hz and synchronized to the shared simulation clock across Unity and VISSIM, enabling millisecond-level alignment between neural responses and in-simulation

events such as cut-ins or braking maneuvers.

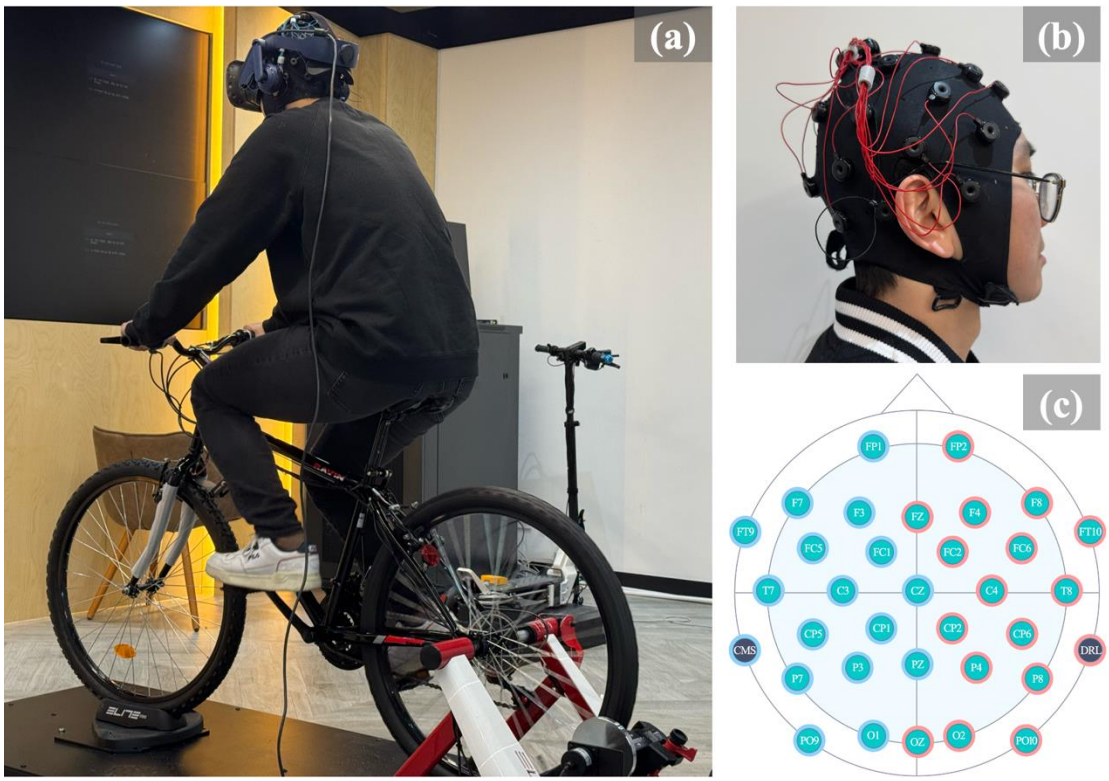

Figure 3 Apparatus (a) bike simulator with EEG cap & VR headset; (b) EEG cap; (c) EEG channels

3.2.2. Participants and procedure

72 participants (47 males and 25 females) aged 18 - 48 years (M = 26.64, SD = 5.24) representing diverse nationalities were recruited from varied professional backgrounds, including students, engineers, and designers. Demographic data, including gender, age, and nationality, were collected (detailed in Table 1), and participants self-identified their cyclist type based on Dill and McNeil (2013): Strong and Fearless, Enthused and Confident, Interested but Concerned, and No Way No How. This stratification supported the examination of behavioral and neural variability across cyclists' profiles, reinforcing the robustness of subsequent analytical models.

The experiment was conducted between December 2024 and February 2025, following approval by the University Human Research Ethics Committee (Protocol No. KH2024-260). Upon arrival, participants signed an IRB-compliant informed consent form and received standardized instructions. They were asked to operate the bicycle simulator according to their usual cycling habits and to avoid collisions with motorized traffic, adhering to real-world traffic rules. Before the formal experiment, a 5-minute adaptation session allowed participants to practice using the simulator and familiarize themselves with the VR environment.

A between-subjects design (Ullmann *et al.* 2022) was used, with thirty-six participants assigned to either the high or low traffic volume condition, ensuring balanced distributions of gender, nationality, and age across groups. To mitigate potential trial order effects, scenario sequences were randomized using a computer-generated Latin square, and a double-blind procedure prevented participants and experimenters from anticipating the sequence (Ma *et al.* 2024). Traffic flows were generated in VISSIM using a fixed random seed to ensure consistent baseline vehicle behaviors, particularly in car-following dynamics and speed distributions. Participants' real-time cycling actions, such as changes in speed or lateral positioning within the lane, influenced surrounding vehicle behavior by affecting following distances and overtaking decisions. This setup allowed human-vehicle interactions and conflict events to emerge naturally based on participants' behavior rather than being pre-scripted.

Before each scenario, participants underwent a baseline EEG calibration consisting of 30 seconds of eyes-open and 30 seconds of eyes-closed resting-state recording. These baseline data

were later used for independent component analysis (ICA) to remove ocular artifacts (Ma *et al.* 2024). Between trials, a two-minute self-paced rest period was provided, accompanied by a natural landscape VR scene to mitigate cognitive fatigue. Throughout the experiment, participants who reported symptoms of simulator sickness, such as nausea or dizziness, had their sessions temporarily paused and were given the option to withdraw if needed.

3.3. Synchronization of TTC, EEG data, and BE features

3.3.1. Time-to-Collision (TTC) extraction and conflict segment identification

TTC refers to the estimated time remaining until a collision occurs, assuming constant speeds for both the cyclist and the following vehicle (Campisi *et al.* 2020). It serves as a safety measure of the potential crash risk between the cyclist and surrounding vehicles, and was calculated using trajectory data obtained from VISSIM. During the VR experiment, VISSIM continuously tracked the positions of all surrounding vehicles at a 100-ms interval. The relevant following vehicle was defined as the one in the same lane with the shortest longitudinal distance to the cyclist. TTC was estimated as in Equation 1:

$$TTC = \frac{\Delta d}{\Delta v} \tag{1}$$

where Δd denotes the longitudinal distance between the front position of the following vehicle and the rear boundary of the cyclist's rigid-body model in VISSIM. Δv indicates the relative velocity and is calculated as the speed of the following vehicle minus that of the cyclist. If the following vehicle's speed was less than or equal to that of the cyclist, TTC was considered infinite, indicating no potential collision risk.

Conflict segments were identified as continuous periods during which TTC remained less than 3 seconds (Darzian Rostami *et al.* 2020). A conflict segment was initiated when TTC first fell to 3 seconds or below and ended when the relevant following vehicle yielded or overtook the participant. To ensure each sample met the minimum temporal length required for subsequent model training, conflict segments shorter than 2 seconds were excluded, resulting in 1,446 conflict segments. These segments were categorized into different maneuver types according to different risk exposure patterns and their potential to trigger divergent psychological responses (Aldred 2016, Kovaceva *et al.* 2019). Specifically, three conflict events were defined based on whether the cyclist was overtaken by a lead vehicle within the preceding two seconds and the following vehicle's subsequent interaction pattern. “Overtaken and tailgated” events, accounting for 61% of cases, occurred when the cyclist was initially overtaken, after which the following vehicle decelerated to maintain a period of car-following state rather than immediately attempting to overtake. “Successive overtaken” events (16%) referred to instances where, following a lead vehicle's overtake, the cyclist was successively overtaken by the following vehicle that maintained its speed without decelerating. The remaining 23% were classified as “non-overtaken” events, in which no lead vehicle overtakes occurred within the preceding two seconds.

3.3.2. EEG signal processing and relative Alpha (α) power calculation

To quantify cyclists' perceived safety, raw EEG signals were transformed into relative alpha power (Bogacz *et al.* 2021). EEG data were recorded at a sampling rate of 256 Hz using the EMOTIV EPOC Flex system, and preprocessing was conducted in MATLAB using the EEGLAB toolbox.

To remove physiological and environmental artifacts (e.g., eye blinks and muscle activity), the signals were bandpass filtered from 0.5 to 30 Hz using zero-phase high-pass and low-pass FIR filters (Zhang and Yan 2023). Independent Component Analysis (ICA) was then performed to isolate and reject artifact components based on their temporal, spectral, and topographic properties (Ma *et al.* 2024). Eye-blink components were identified using the ADJUST plugin, and outlier channels were interpolated using spherical spline interpolation (Ma *et al.* 2024). Baseline correction was applied using the resting state EEG (eyes-open and eyes-closed conditions) collected prior to the experimental tasks.

For frequency-domain analysis, continuous EEG data were divided into 256-sample segments with a 26-sample sliding step and processed using a Hanning-windowed fast Fourier transform (FFT) to estimate power spectral density (PSD), with 1 Hz frequency resolution. Each spectral estimate was time-stamped to the center of its analysis window and used for temporal alignment with TTC data. PSD values were computed within the 0.5–30 Hz range, encompassing the standard EEG frequency bands: δ (0.5–4 Hz), θ (4–8 Hz), α (8–13 Hz), and β (13–30 Hz). Absolute α power was derived by averaging PSD values across the 8–13 Hz band. To reduce individual differences in total power and facilitate across-subject comparison, relative α power was computed as the ratio of alpha power to the total power within the 0.5–30 Hz range (Zhang and Yan 2023).

3.3.3. Extraction of BE features

Video recordings corresponding to conflict segments were sampled at 100-millisecond intervals, yielding 57,481 frames for BE feature extraction. Features were derived using semantic

segmentation, with visual complexity further quantified to reflect BE spatial organization. The selection and summary of BE features are adapted from (Xu *et al.* 2025) and presented in Table 1.

The semantic segmentation process utilized a deep learning pipeline developed by CSAILVision (https://github.com/CSAILVision/semantic-segmentation-pytorch), combining a ResNet50-dilated encoder and PPM_deepsup decoder pretrained on the ADE20K dataset (Zhou *et al.* 2019). This model effectively identified key street-level BE elements such as buildings, sky, walls, trees, roads, pavements, greenery, and streetlamps. Prior studies have validated the high accuracy of this segmentation approach in visual parsing tasks and its compatibility with VR environments (Luo *et al.* 2025). Figure 4 demonstrates the reliable performance in extracting BE features, where extracted greenery and vehicle pixel ratios specifically exhibited strong positive correlations with the pre-set greenery coverage (Spearman's $r = 0.86$, $p < 0.001$) and traffic volume levels (Spearman's $r = 0.83$, $p < 0.001$), respectively. This high correlation confirms the effectiveness of capturing variations in experimental scenarios, translating static settings into high-temporal-resolution basis for subsequent model development.

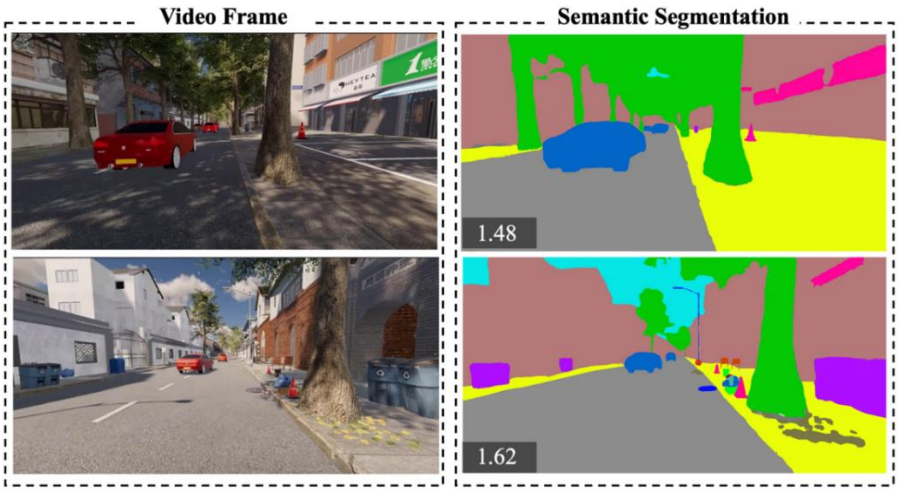

Figure 4 Results of semantic segmentation and feature diversity

Three indicators were used to quantify visual complexity: feature diversity, texture complexity, and color entropy. Feature diversity (Figure 4) was computed from semantic segmentation outputs using a Shannon entropy-based measure (Ma *et al.* 2023), as shown in Equation 2:

$$vis\_feature = -\sum_{i=1}^{N} p_i log\, p_i \quad (2)$$

where N represents the number of segmented feature types, p_i is the proportion of pixels belonging to the i^{th} in each frame.

Texture complexity was assessed via a fractal-based method (Ma *et al.* 2023). After applying Canny edge detection, the resulting edge maps were analyzed using the box-counting approach to compute the slope of the log–log curve, yielding the Visual Complexity of Texture (vis_texture), as shown in Equation 3:

$$vis\_texture = \lim_{\varepsilon \to 0} \frac{logN(\varepsilon)}{\log\left(\frac{1}{\varepsilon}\right)} \quad (3)$$

where $N(\varepsilon)$ refers to the number of boxes of size ε is the side length of the boxes.

In parallel, the variation in color (Figure 5) was assessed using grayscale spatial entropy (Guan *et al.* 2022), presented in Equation 4.

$$vis\_color = -\sum_{i=0}^{255} \left(p_i log_2 p_i + \sum_{j=0}^{255} p_{ij} log_2 p_{ij} \right) \quad (4)$$

where p_i indicates the proportion of pixels with the grayscale value i in each frame ($0 \leq i \leq 255$), p_{ij} indicates the proportion of pixels with a grayscale intensity of i, which are spatially adjacent to pixels exhibiting an average grayscale intensity of j within each frame.

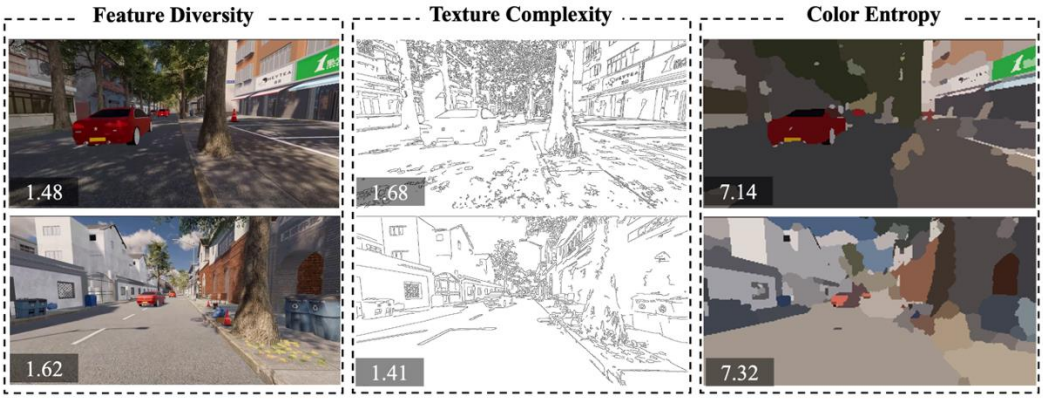

Figure 5 Results of feature diversity, texture complexity and color entropy

Table 1 Feature selection and data description

Features	Description	Min	Max	Mean	SD
BE features	Extracted from 57,481 frame images				
Greenery	Proportion of pixels classified as trees and vegetation	0	0.66	0.14	0.09
Sky ratio	Percentage of pixels identified as sky in the frame	0	0.86	0.04	0.05
Vehicle ratio	Fraction of pixels segmented as vehicles in the field of view	0	0.21	0.02	0.03
Enclosure	Proportion of lateral field of view enclosed by buildings, trees, and walls	0	0.91	0.53	0.11
Feature diversity	Shannon entropy of segmented BE feature distributions	0.02	2.21	1.45	0.18
Texture complexity	Fractal dimension of edge-based texture	1.13	1.76	1.42	0.21
Color entropy	Gray-level Co-occurrence matrix entropy	0.31	7.75	7.30	0.97
Perceived safety					
Relative α wave	Higher values indicate greater perceived safety	0.06	0.53	0.24	0.12
Actual potential risk					
TTC		0.14	3.00	0.83	0.73
Conflict segment events		1446			
Overtaken and tailgated events		882			
Successive overtaken events		234			
Non-overtaking events		330			
Demographic features		N (participants)			
Cyclist type					
No way no how: not interested in cycling		14			
Interested but concerned: unwilling to bike next to fast traffic or on busy roads		32			
Enthused and confident: willing to tolerate busy traffic if there is designated space for bicycles		22			
Strong and fearless: insensitive to traffic conditions		4			
Nationality					
Chinese		38			
Non-Chinese		34			
Gender					
Male		47			
Female		25			
Age Group					
18-28		48			
29-38		16			
39-48		8			

3.4. LSTM model development and interpretation

3.4.1. LSTM architecture for relative α wave prediction

LSTM model was chosen for its strength in modeling temporal dependencies in cyclists' neural responses. In this study, relative α wave patterns evolve in response to continuous environmental stimuli and require capturing both short-term reactions and longer-term contextual effects. LSTM's ability to retain and integrate information across time steps makes it particularly suitable for this context, where moment-to-moment variation in visual information may have delayed or cumulative impacts on people's neurophysiological responses (Galpin *et al.* 2009, Zhang *et al.* 2020). This temporal sensitivity offers a robust foundation for data-driven investigation of perception-risk mismatches under varying traffic scenarios.

To investigate from a data-driven perspective whether BE features influence cyclists' perception of actual potential risk, two LSTM-based models were developed to predict relative alpha power as a proxy for perceived safety. Both models utilized time-series segments extracted from 1,446 identified conflict segments, with each spanning 1 second and sampled every 0.1 second, yielding 10-frame sliding windows. The first model, LSTM-base, included only TTC and sociodemographic features. The second model, LSTM-BE, expanded upon this by incorporating BE-related inputs.

Each frame in LSTM-BE included 13 input features: 8 continuous variables (TTC and 7 BE features), 4 categorical variables (sociodemographic), and one temporal encoding indicating the frame's position within the segment. In contrast, LSTM-base excluded BE features, resulting in 6 inputs: TTC, the same 4 categorical variables, and the temporal encoding. All features were

normalized using min-max scaling. The dataset was split into training, validation, and testing sets in a 7:2:1 ratio, yielding 40,236 training, 11,496 validation, and 5,749 testing samples.

The model architecture is illustrated in Figure 6. It begins with two parallel fully connected layers designed to process continuous and categorical features separately, while temporal features are directly incorporated and subsequently concatenated with the outputs from both branches. This merged representation is passed through a 32-unit fully connected fusion layer and then through two stacked LSTM layers that learn temporal dependencies. The two stacked LSTM layers consist of 32 and 16 hidden units, respectively, with no dropout applied. The hidden state at the final time step is extracted and processed through a final fully connected layer that outputs one value representing the predicted relative α wave. The model is trained by minimizing mean squared error using the Adam optimizer (Zhang *et al.* 2020) with a weight decay of 0.1. The learning rate is 0.001, with β_1 is 0.9, β_2 is 0.999, ϵ is 1e-8. All implementations are carried out using the PyTorch framework.

To validate the necessity of the proposed LSTM architecture, four baseline models were developed, and all methods were evaluated under identical data settings for both feature sets (base and BE). Specifically, comparisons were made against (i) Linear Mixed Models (LMM) to account for individual variability, (ii) Random Forest (RF) to capture non-linear but non-temporal relationships, (iii) a fully connected deep neural network (DNN), and (iv) a standard recurrent neural network (RNN) to isolate the effect of LSTM gating. All models used the same training, validation and test data split and identical hyperparameter tuning strategy. For sequence-based models (RNN, and DNN), inputs were consistent with the LSTM setting; the RNN processed the 10-time steps

sequentially, while the DNN consumed the same window without recurrent states. In contrast, since LMM and RF cannot directly model temporal dependencies, each 10-frame window was summarized by averaging frame-level features over time and treated as one independent observation. The RF was implemented in scikit-learn with 100 trees and no maximum depth. The DNN consisted of three hidden fully connected layers (128, 64, and 32 units) with ReLU activation, and the RNN adopted a hidden-state configuration aligned with the LSTM for a fair comparison.

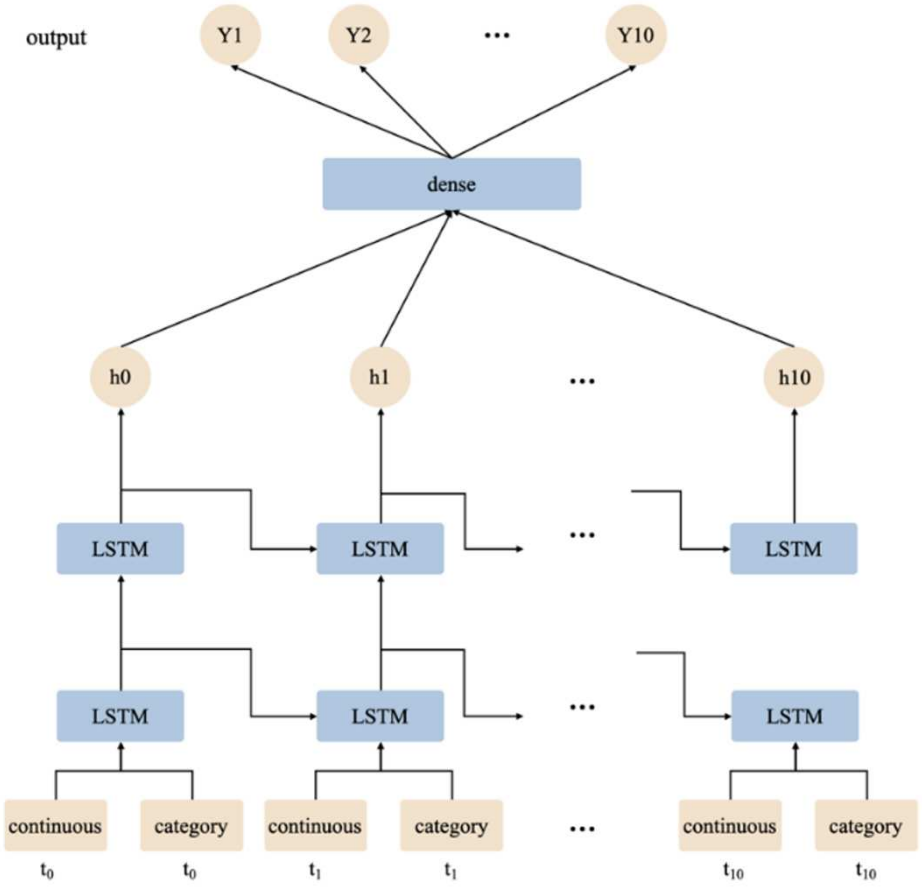

Figure 6 LSTM model architecture

3.4.2. Model interpretation analysis

Partial Dependence Plot (PDP) was leveraged to examine how individual input features influence the model's predicted perceived safety by isolating their marginal effects. Given that deep

learning models often lack interpretability due to their black-box nature, PDP provides a model-agnostic way to approximate and visualize feature impacts (He *et al.* 2024). This study iteratively fixed a selected feature x_s across a uniform range of values observed in the training set. For each fixed value, all instances of x_s across the entire time sequence have been placed in the input tensor, while keeping the remaining features x_c unchanged. The trained LSTM model then predicted the relative α wave based on these modified inputs. The average prediction was computed for each value of x_s, yielding the PDP curve. The process was repeated across five cross-validation folds, and the average result was reported. The formal expression for PDP estimation is shown in Equation 5:

$$f(x_s) = \mathbb{E}_{x_c}[f(x_s, x_c)] \approx \frac{1}{n}\sum_{i=1}^{n} f\left(x_s, x_c^{(i)}\right) \quad (5)$$

where n is the number of sampled instances, and $x_c^{(i)}$ is the complement feature set for the i^{th} instance.

To further examine the features that modulate cyclists' perception of actual potential risk, Friedman's H-statistic (Friedman and Popescu 2008) was applied, with higher values indicating stronger interaction effects. This statistic measures the degree to which the joint effect of two features on the model output deviates from the sum of their independent effects (Equation 6).

$$H^2 = \frac{\mathbb{E}[(f(x_s, x_t) - f(x_s) - f(x_t) + f_0)^2]}{\mathbb{E}[f(x_s, x_t)^2]} \quad (6)$$

Where $f(x_s, x_t)$ is the joint partial dependence, $f(x_s)$ and $f(x_t)$ are the univariate partial dependencies, and f_0 is the average model prediction. The final H-statistic is computed by comparing the variance of the full interaction surface to the variance explained by the additive

components.

4. Results and Discussion

4.1. Model performance

Table 2 presents the comparative performance of the baseline models and the LSTM architecture, evaluated on two feature sets: ‘base’, which incorporates only sociodemographic features and TTC, and ‘BE’, which includes BE features in addition to these inputs. Results demonstrate that the LSTM architecture outperformed all baseline approaches across both feature sets. Notably, the LSTM-BE model yielded the lowest error rates among all tested configurations (Test MSE = 0.0089). Furthermore, the distribution of prediction errors (Appendix 7.1, Figure A.1) reveals that the MSE loss remains stable across different TTC spectrums, validating the model's reliability in high-risk scenarios. This superior performance over both static and simpler sequence models underscores that perceived safety is a cumulative cognitive process dependent on temporal context, rather than a mere response to instantaneous stimuli. Furthermore, the significant performance improvement of LSTM-BE over LSTM-base confirms the hypothesis that perceived safety is not solely determined by objective risk, but is significantly modulated by BE features (Ye *et al.* 2024).

Table 2 Model Performance Comparison

Model		**Training set**	**Test set**		
		MSE	**MSE**	**MAPE**	**MAE**
Linear Mixed Model (LMM)	LMM-base	0.0435	0.0443	64.37%	0.15
	LMM-BE	0.0328	0.0331	61.27%	0.15
Random Forest (RF)	RF-base	0.0352	0.0245	40.12%	0.12
	RF-BE	0.0145	0.0133	28.50%	0.09
Deep Neural Network (DNN)	DNN-base	0.0426	0.0322	45.47%	0.14
	DNN-BE	0.0242	0.0244	39.42%	0.12
Recurrent Neural Networks (RNN)	RNN-base	0.0378	0.0273	42.29%	0.13
	RNN-BE	0.0221	0.0216	37.99%	0.12
Long Short-Term Memory (LSTM)	LSTM-base	0.0339	0.0208	38.63%	0.11
	LSTM-BE	**0.0101**	**0.0089**	**22.59%**	**0.07**

4.2. Marginal effects between TTC and perceived safety

PDPs (Figure 7) show the marginal effect of each variable on the predicted relative α wave, which increases with perceived safety and decreases under heightened caution. The 5-fold validation bands demonstrate model stability, with narrower deviations suggesting robust pattern capture. Critically, these PDPs represent the average marginal effects across the population, as defined by the machine learning interpretability framework (Molnar, 2020). They characterize how the model systematically associates TTC variations with perceived safety changes, rather than depicting time-dependent physiological responses of individual cyclists.

An apparent mismatch emerged between cyclists' perceived safety and actual risk at very low TTC values (Figure 7). The PDP of the denormalized TTC revealed that cyclists' perceived safety remained stable where TTC value from 3s to 1.8s, consistent with existing literature suggesting cyclists typically recognize risks around a 2s TTC (Rasch *et al.* 2020). As TTC decreased from 1.8s to 0.6s, perceived safety intuitively declined due to escalating threats. However, below 0.6s TTC, a

paradoxical increase in relaxation occurred among cyclists, contradicting linear expectations of risk perception and underscoring the need to investigate underlying cognitive and environmental mechanisms.

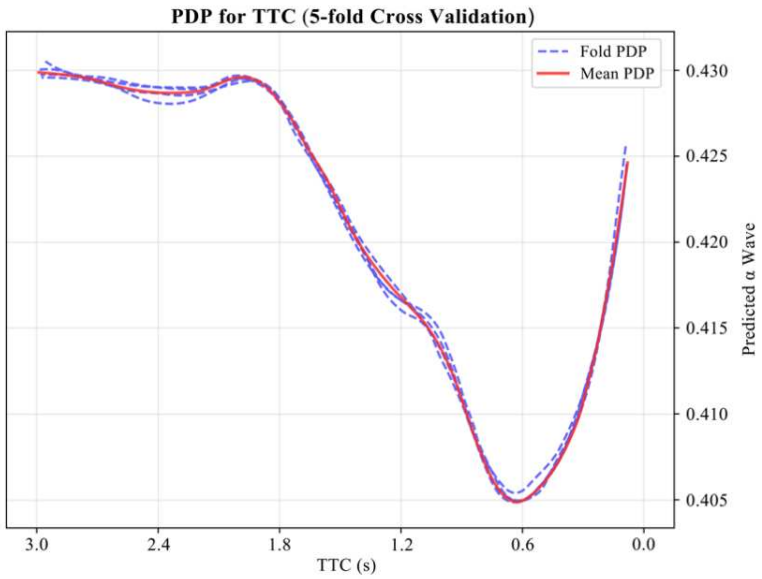

Figure 7 PDP of TTC on perceived safety

Since overtaken and tailgated events (61%), successive overtaken events (16%), and non-overtaken events (23%) within the dataset involve fundamentally distinct risk exposure patterns and psychological responses (Aldred 2016, Kovaceva *et al.* 2019), stratified PDP analyses were performed for each conflict type to verify the consistency of the identified mismatch phenomenon (Figure 8). Results indicated an intuitive declining safety perception with decreasing TTC in both non-overtaken and successive overtaken events. In contrast, the paradoxical relaxation at extremely low TTC levels occurred exclusively in overtaken and tailgated events, confirming the specificity of the mismatch phenomenon to the car-following status immediately following an overtaking maneuver.

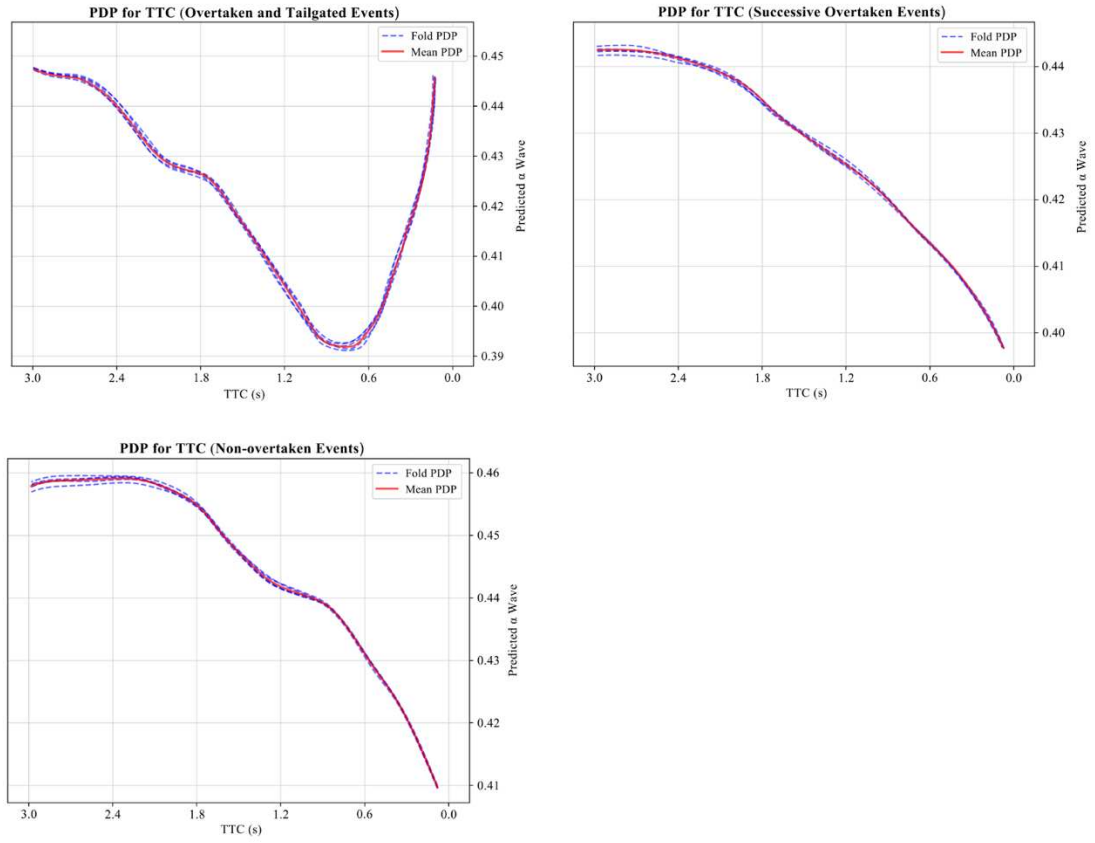

Figure 8 Stratified PDP of TTC on perceived safety by conflict events

To further investigate the mismatch phenomenon in the overtaken and tailgated events, temporal dynamics involving α waves, TTC, and inter-vehicular distances were systematically analyzed (Figures 9 and 10). Figure 9 presents the median trends with Interquartile Ranges (25th–75th percentiles) derived from aggregated conflict segments, marked with representative interaction scenarios between the lead vehicle, following vehicle, and cyclist. Here, positive vehicle distance indicates an approach from the rear, while negative distance denotes the vehicle has overtaken the cyclist. As the lead vehicle initiates the maneuver and enters the cyclist's forward field of view (scenario a in Figure 9-10), relative α power drops to its minimum, reflecting peak tension. Subsequently, the lead vehicle completes the pass (scenario b in Figure 9-10). At this moment, the following vehicle continues to close in (median distance: 12.3 m; SD: 7.6 m; IQR: 10.21–34.57 m)

and proceeds to maintain a car-following state (scenario b-c in Figure 9-10). However, despite the persistently low TTC, relative α power exhibits a sustained rebound. This phenomenon, occurring as the gap between the lead and following vehicles progressively widens, aligns with the counter-intuitive relaxation observed in the PDP analysis (TTC < 0.6 s). This suggests that cyclists experience temporary relief after the immediate visual threat has passed, momentarily overlooking the subsequent risk posed by approaching vehicles.

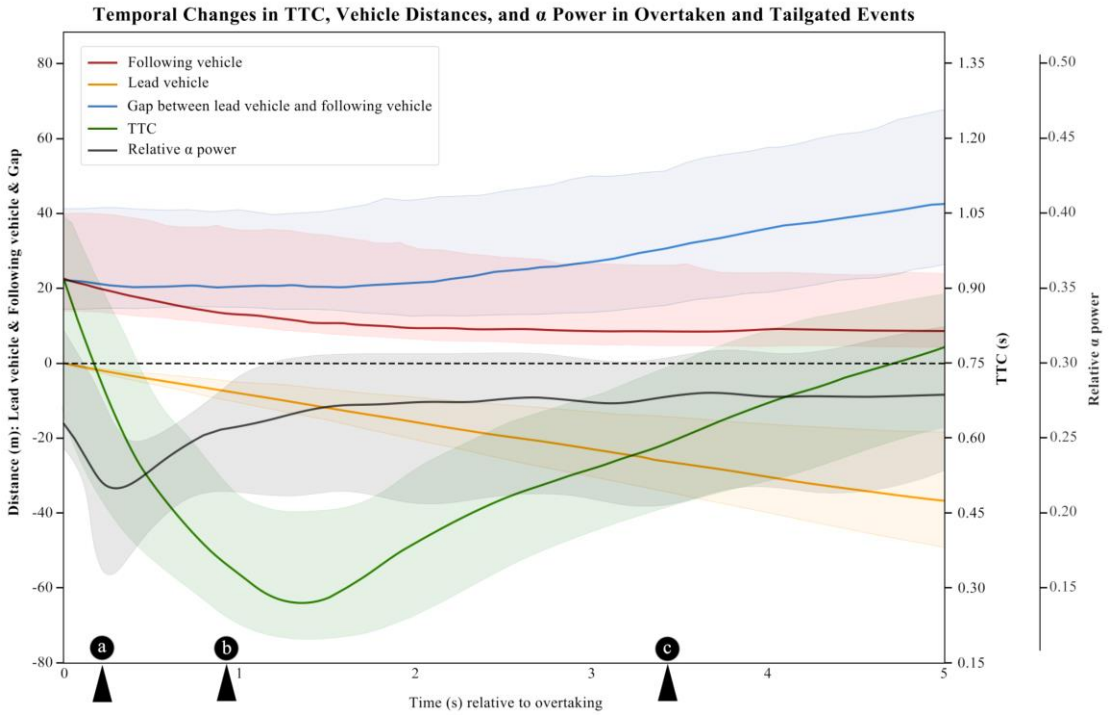

Figure 9 Temporal changes in TTC, inter-vehicular distance and α wave in overtaken and tailgated events; representative interaction scenarios include (a) the lead vehicle entering the cyclist's forward field of view, (b) the lead vehicle completing the pass, and (c) the lead vehicle accelerating away.

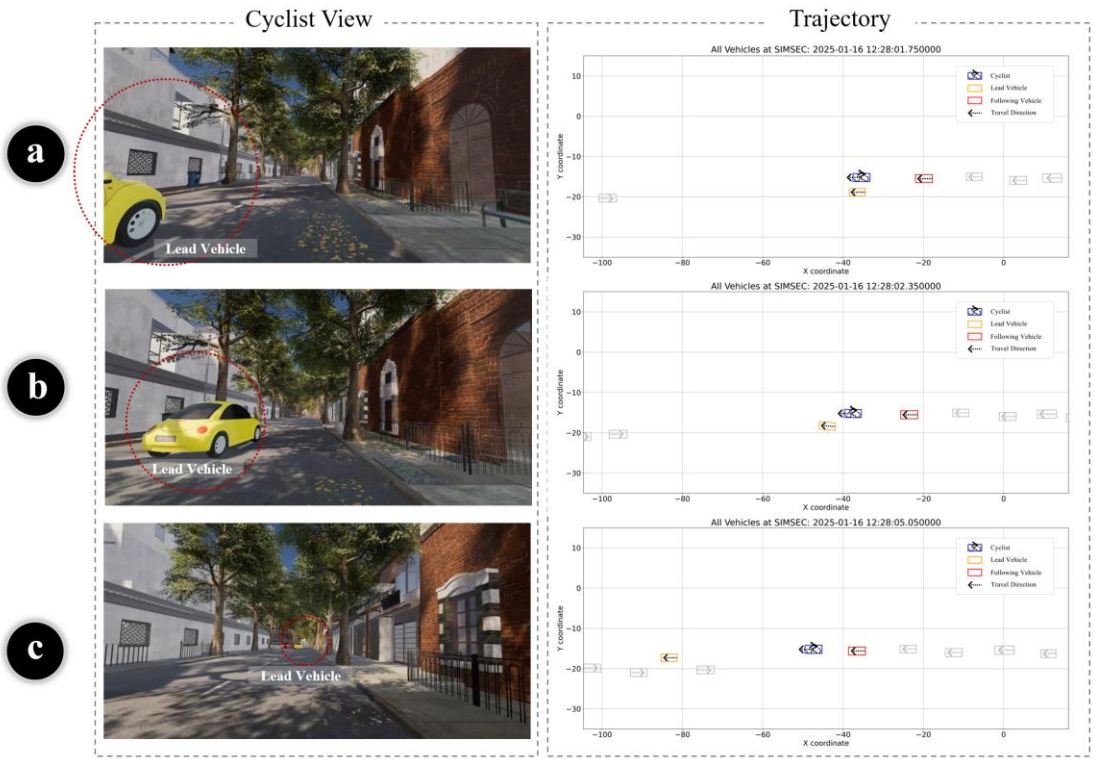

Figure 10 Cyclist view and vehicle trajectories across representative interaction scenarios

To distinguish whether the observed relaxation involves sustained risk awareness or merely a physiological rebound, the topographic distributions (Figure 11) of α activity were analyzed alongside θ and β bands, which serve as neural markers for cognitive processing and attentional control (da Silva *et al.* 2022). EEG recordings were segmented into two event-related phases: a during-overtaking phase, spanning from the initiation of the overtake (prior to scenario a in Figure 10) to its complete passage (scenario b in Figure 10); and an after-overtaking phase, with the analysis window determined by the average duration of the identified mismatch phase within the conflict segments (scenario b-c in Figure 10). Relative spectral power changes were calculated and normalized against the reference interval immediately preceding the vehicle's approach.

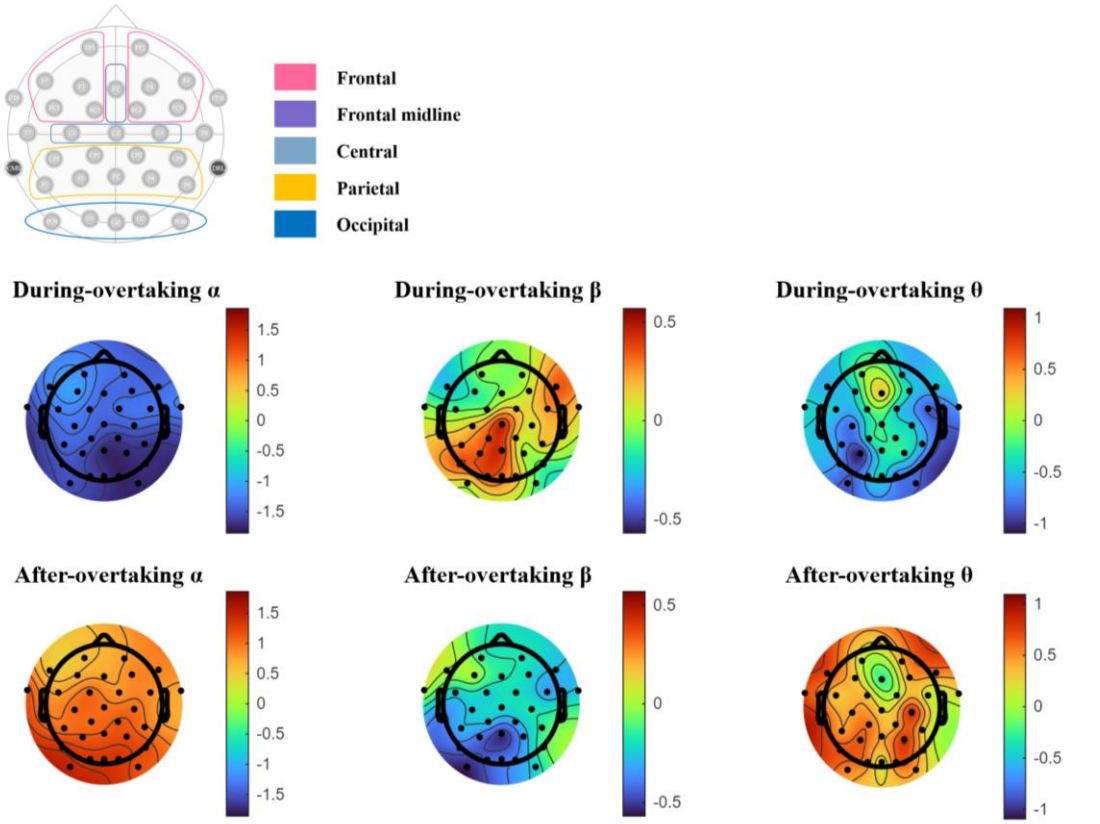

Figure 11 Topographic distributions of relative spectral power changes (in dB) across α, β and θ bands

The topographic distributions (Figure 11) reveal distinctly contrasting neural patterns between the two event phases, suggesting a transition from heightened vigilance to a state of potential cognitive disengagement immediately following the overtaking maneuver. During the overtaking phase, the brain exhibited a state of high alertness and stress response compared to the reference interval. Specifically, α power showed widespread suppression, most pronounced in the parieto-occipital regions, a pattern classically associated with increased visual attention and external vigilance (Magosso *et al.* 2019, Bacigalupo and Luck 2022). Concurrently, β power surged across parietal and occipital areas, indicating active engagement in hazard monitoring (Li *et al.* 2022),

while a localized reduction in left-frontal β activity aligned with neural signatures of acute stress and fear processing (Kim *et al.* 2017, Roxburgh *et al.* 2023). Furthermore, θ power generally decreased while a synchronization pattern emerged along the frontal midline, suggesting intensified executive control and conflict monitoring in response to the uncertainty of the approaching vehicle (Yamada 1998, Roxburgh *et al.* 2023). In contrast, the after-overtaking phase was characterized by neural markers of relaxation and attentional withdrawal, aligning with the 'stress fatigue' observed in early driving simulations where acute tension induces temporary exhaustion and reduced vigilance (Heimstra 1970). This shift is evidenced by a global resurgence of α and general θ power, accompanied by distinct suppression in parieto-occipital β and frontal midline θ activity. While this neural pattern signifies the restoration of psychological homeostasis, it suggests a functional shift toward the Default Mode Network (DMN), a state synonymous with mind-wandering and reduced sensitivity to external environments (Wascher *et al.* 2014, Van Son *et al.* 2019, Arnau *et al.* 2020, Conrad and Newman 2021, da Silva *et al.* 2022).

This neural signature of rapid attentional withdrawal aligns with the psychological response typical of "near-miss" events, which involve close encounters that do not result in physical harm (Aldred 2016). Aligning with prior research, overtaking maneuvers are initially perceived as near misses that significantly elevate cyclists' stress and tension (Llorca *et al.* 2017, Rasch *et al.* 2022). However, when no harm subsequently occurs, individuals often exhibit a paradoxical shift from acute fear to pronounced relief, gratitude, or a sense of luck, a pattern that mirrors the relaxation observed in the present study (Teigen 1997, Teigen and Jensen 2010, Terum and Svartdal 2019). This transition arises because, when facing an imminent threat, individuals tend to generate dramatic

downward counterfactuals, imagining outcomes worse than those actually experienced (Teigen 1995, 2005, Terum and Svartdal 2019). Such cognitive processes explain why people frequently feel relief or even mild euphoria following near misses, interpreting them as escapes or fortunate outcomes (Teigen 1995). However, the neural data indicate that this relief reflects an emotional response rather than a rational reassessment of risk. This perceptual relief creates a hazardous temporal window in which cyclists, reassured by the passing of the primary threat, may neglect subsequent dangers, thereby elevating the risk of secondary accidents due to delayed threat detection.

4.3. Influence of BE features and sociodemographic variables

Marginal effects of other variables (Figure 12) exhibit trends consistent with previous literature, supporting the robustness of model interpretations. Greenery, enclosure, and feature diversity exhibited an inverted "V" shape, aligning with findings from previous studies (Bjerke *et al.* 2006, Jiang *et al.* 2015, Kawshalya *et al.* 2022). These features initially enhance perceived safety by fostering relaxation and clearly defining spatial boundaries. However, beyond optimal thresholds, their beneficial effects decline or reverse due to increased complexity and cognitive demands. For instance, Stress Reduction Theory (Ulrich *et al.* 1991) posits that green landscapes facilitate stress recovery (Jiang *et al.* 2014) and are associated with enhanced perceived safety and positive mood (Jiang *et al.* 2017, Xu *et al.* 2025), which is consistently supported by empirical driving research (Jiang *et al.* 2021). However, excessive greenery transitions from a restorative factor to a source of psychological stress by obstructing sightlines, aligning with findings from previous studies (Asgarzadeh *et al.* 2012, Ye *et al.* 2024). Furthermore, high-density vegetation may trigger vigilance

due to 'real-world inertia,' where cyclists instinctively perceive dense foliage as concealing potential threats, such as pedestrians suddenly emerging, even though they were informed that the simulation was pedestrian-free. Similarly, vehicle density displays a tolerance threshold where cyclists feel comfortable navigating alongside moderate traffic flow, suggesting that the predictability of vehicle movements and sufficient inter-vehicle headway afford cyclists adequate reaction time (Teh *et al.* 2014). However, this perception deteriorates precipitously once the volume exceeds a tipping point, overwhelming the cyclist's cognitive capacity to monitor continuous dynamic threats.

Sky ratio consistently demonstrated a negative effect on perceived safety, stabilizing at higher exposure levels likely due to increased feelings of vulnerability in open environments. Contrary to previous studies that suggest moderate diversity in texture and color entropy can enhance perceived safety, this study found continuous adverse effects (Ewing and Handy 2009, Kawshalya *et al.* 2022). This discrepancy may be attributed to differences in context, particularly between general environments previously studied and the high-risk scenarios examined here.

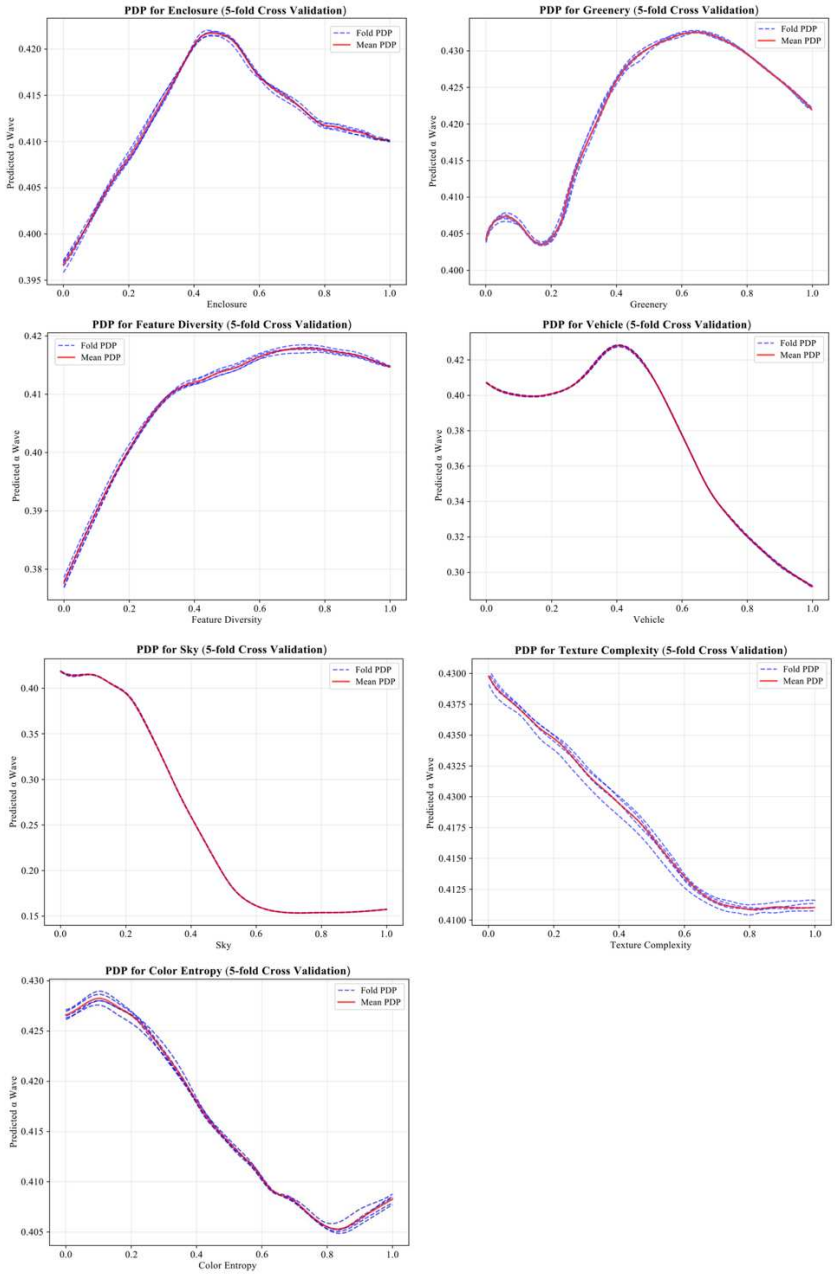

Figure 12 PDP of BE features on perceived safety

Regarding sociodemographic variables (Figure 13), findings aligned with extensive literature, noting that females exhibited greater anxiety than males, nervousness increased with age, and Chinese participants reported greater relaxation due to environmental familiarity (Zeuwts *et al.* 2017, Griffin *et al.* 2020). Interestingly, cyclist type presented counterintuitive outcomes; "no way, no

how" cyclists expressed similar perceived safety levels as "enthused and confident" cyclists (Dill and McNeil 2013). This might be attributable to their frequent use of alternative transport modes (e.g., vehicles or e-scooters), enhancing their perceived control and confidence during cycling activities.

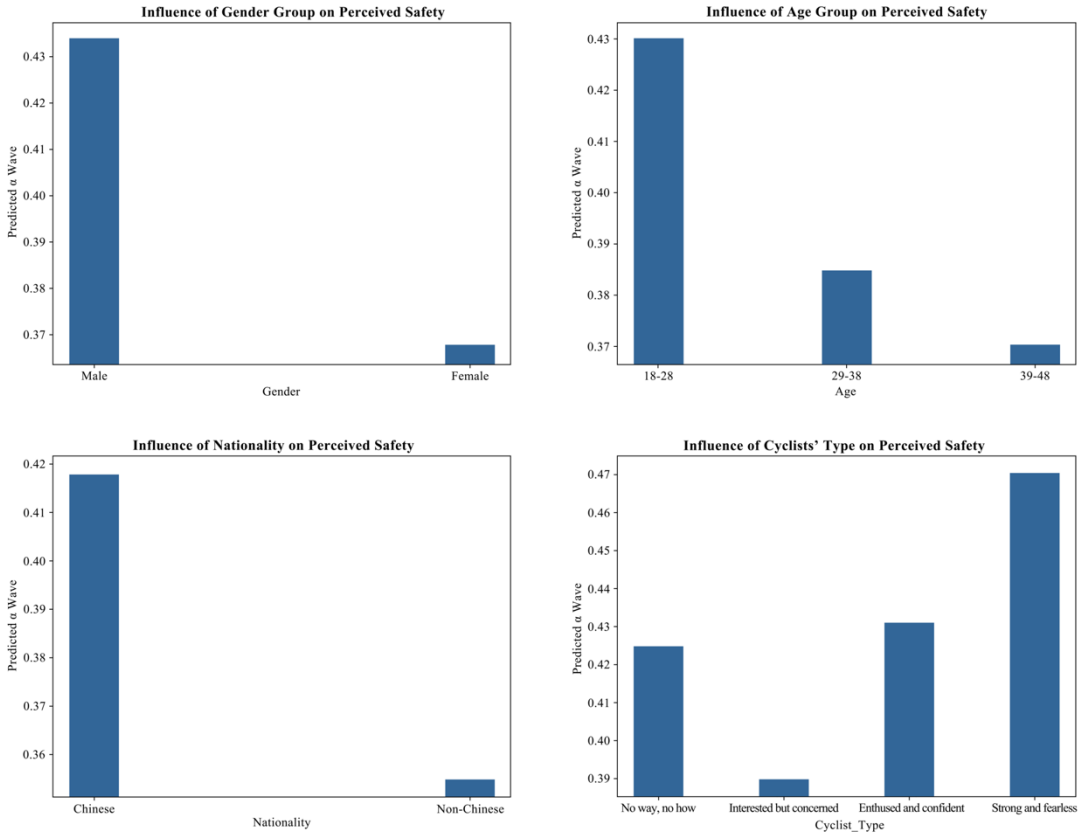

Figure 13 Influence of demographic features on perceived safety

4.4. Built Environment features amplifying mismatch

Friedman's H-statistic was applied to evaluate interactions between TTC and other variables collectively contributing to overtaking mismatch scenarios. Figure 14 illustrates these interactive intensities, with values exceeding 0.5 indicating strong interactive effects warranting deeper analysis (Friedman and Popescu 2008). To ensure the reliability of these interactive effects, the

prediction error distributions across the corresponding feature combinations were examined (Appendix 7.1, Figures A.2–A.6). The results reveal a generally uniform error distribution, confirming that the model maintains consistent predictive capability across these complex feature combinations without systematic bias.

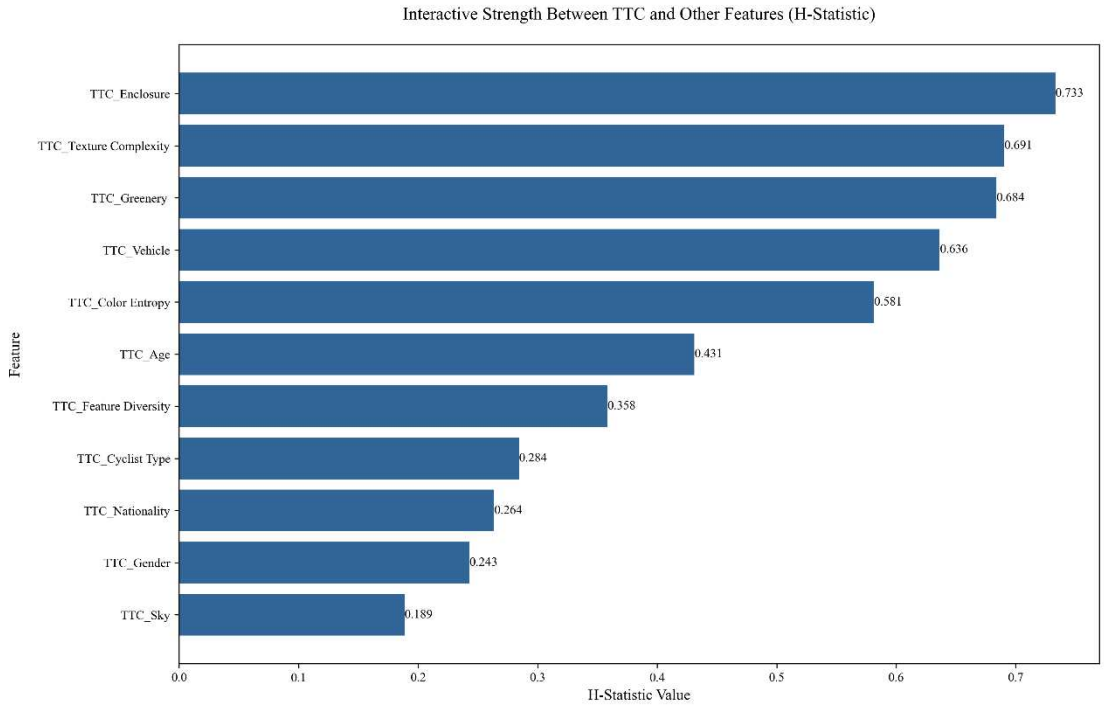

Figure 14 Interaction effects between TTC and other features based on H-Statistic analysis

As shown in Figure 15, the interaction analysis focuses on mismatch segments where TTC falls below 0.6 seconds, aiming to reveal how key BE features amplify perception–risk mismatch. Significant interactions were identified for enclosure, texture complexity, greenery, vehicle proportion, and color entropy. Contrary to the marginal effects observed in the PDP analysis, high levels of enclosure, texture complexity, color entropy, and greenery were associated with elevated perceived safety during these high-risk intervals. This paradox suggests that these seemingly beneficial BE features, however, may unintentionally intensify the mismatch between perceived

safety and actual risk in critical situations.

This phenomenon can be explained by the change of cognitive resources and the shift in attentional control. Previous studies indicate that attentional capacity declines following stress-inducing events such as near-misses, causing a shift from top-down to bottom-up attentional allocation (Diarra *et al.* 2023). Although top-down executive control effectively filters out irrelevant visual details under normal conditions, resource depletion following overtaking maneuvers weakens this suppression (Jiang *et al.* 2021). During these periods of cognitive disengagement, high greenery and complex environments act as visually engaging stimuli that capture attention effortlessly, inducing the fatigued brain into a state of deep relaxation and mind-wandering (Ma *et al.* 2023). Given that individuals typically engage in horizontal rather than vertical visual scanning, this heightened environmental complexity may encourage broader peripheral exploration, exacerbating attentional demands (Galpin *et al.* 2009). In addition, a low visible vehicle density indicating sparse traffic flow may generate a false sense of safety, as the absence of continuous visual cues in the forward field of view leads cyclists to underestimate the invisible risk from behind. Therefore, when cyclists attempt to refocus attention on the central visual tasks critical for riding safety, their ability to promptly recognize and respond to new hazards may be significantly impaired.

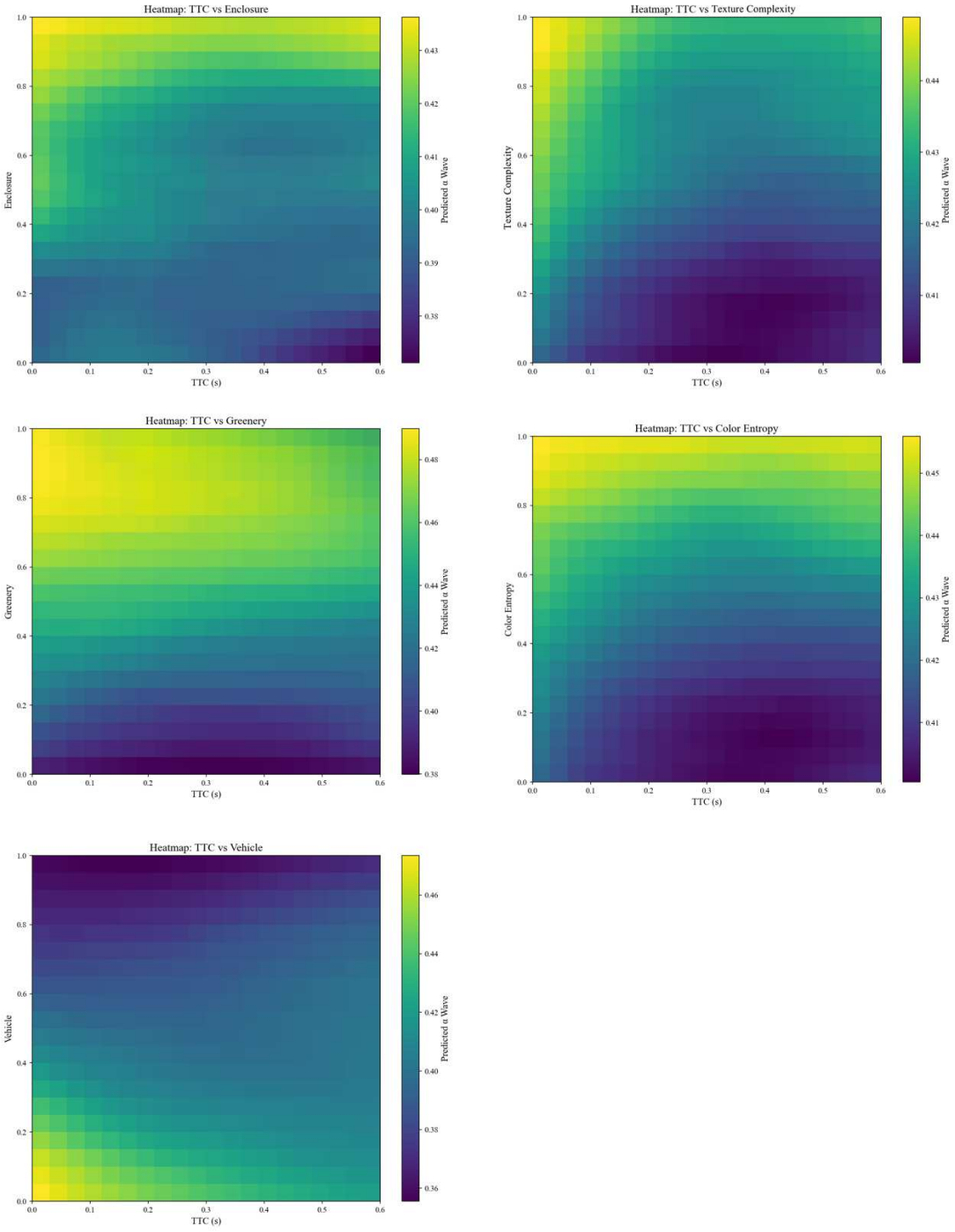

Figure 15 Interactive effects of TTC and key BE features on perceived safety

4.5. Limitation

The study has several limitations. Relative α power was employed as the sole primary proxy

for perceived safety within the EEG spectrum. Compared to the α band, the functional directionality of global β and θ power remains inconsistent. While some empirical studies associate states of reduced attention with power enhancement in these bands (Kar *et al.* 2010, Wei *et al.* 2018, Simor *et al.* 2025), others report power suppression (Braboszcz and Delorme 2011, Van Son *et al.* 2019, Li *et al.* 2022). Therefore, to maintain analytical robustness, these bands were treated as auxiliary topographic indicators rather than linear safety metrics. Additionally, the γ band was excluded from the current analysis due to its high sensitivity to electromyogenic (EMG) contamination inherent to continuous active cycling (Seeber *et al.* 2015). Future research utilizing advanced artifact removal pipelines should aim to integrate these broad spectral components, thereby developing a more comprehensive, multi-band framework for quantifying cyclist safety.

Second, while the VR cycling environment simulated vehicle approach using stereo sound effects, it could not fully replicate the tactile feedback experienced during real-world cycling, such as airflow disturbances and subtle vibrations. Although these sensory cues were absent, the experimental results demonstrated strong consistency across participants, where α wave suppression patterns closely aligned with TTC changes. This suggests that the core mechanisms identified remain robust. Future studies could consider adding calibrated collision warning signals to further enhance the ecological validity of the simulation.

Third, the spatial collision mapping between bicycles and motor vehicles relied on parameterized thresholds rather than fully accurate physical modeling. Although this method could not exactly reproduce real-world contact conditions, such as millimeter-level interactions between

a vehicle's front bumper and a bicycle's rear wheel, the risk gradient patterns derived from the data systematically reflected changes in perceived safety associated with spatial proximity. These patterns exhibited high consistency across scenarios, indicating that the method captured stable and meaningful relationships.

Last, repeated exposure to simulated risk environments may gradually diminish participants' sensitivity to potential risk. As they become increasingly familiar with the VR setting, participants may gain confidence or perceive the scenarios as less threatening due to the awareness that the risks are simulated rather than real. This desensitization effect, along with the possible occurrence of simulator sickness, underscores the need for further validation when attempting to generalize the results to actual traffic environments, as these are limitations commonly observed in simulator-based studies (Kwon *et al.* 2024). A key strength of the current setup, however, lies in its interactivity: participants' real-time cycling behaviors, such as changes in speed or lateral positioning, directly influenced the responses of surrounding vehicles, such as overtaking and maintaining distance. This interactive setup ensured that conflict events emerged organically in response to participants' actions rather than being preset, thereby enhancing the ecological validity of the simulation. To further validate the findings, future research may incorporate real-world road tests or integrate physiological measures, such as galvanic skin response and heart rate, to facilitate cross-validation.

5. Conclusion

This study leveraged a virtual reality (VR) cycling simulation platform integrated with electroencephalography (EEG), computer vision, and VISSIM traffic microsimulation to investigate

the mismatch between cyclists' perceived safety and actual crash risks in dynamic urban environments. A controlled experiment involving 72 participants enabled high-resolution, millisecond-level synchronization across three data dimensions: (1) continuous EEG recordings capturing neural responses related to subjective safety; (2) dynamic extraction of built environment (BE) features (e.g., greenery, vehicle density, visual complexity) from first-person video using computer vision technique; and (3) Time-to-Collision (TTC) metrics derived from traffic simulations to quantify actual potential risks A Long Short-Term Memory (LSTM) model was applied to this multimodal dataset to analyze how discrepancies emerge between perceived safety and potential risk. The results indicate that the mismatch is particularly evident in "overtaken and tailgated" events. Specifically, immediately after being overtaken by the lead vehicle, cyclists temporarily enter a relief phase, during which perceived safety paradoxically rises while potential risks from following vehicles persist. This mismatch is further intensified in environments featuring high levels of enclosure, greater texture and color entropy, dense greenery, and lower visible vehicle ratios.

This study offers several key contributions. First, by integrating synchronized multi-source data, it systematically uncovers the dynamic mismatch between cyclists' perceived safety and objective crash risks, addressing limitations of traditional studies that focus exclusively on either subjective or objective measures. Second, the study's examination of BE feature interactions emphasizes a critical safety paradox: urban design elements intended to enhance aesthetic appeal or emotional restoration may inadvertently increase crash risks in high-conflict road segments by impairing risk perception. Consequently, these findings underscore important policy implications,

highlighting the need to re-evaluate built environment interventions to ensure that aesthetic enhancements are aligned with cyclist safety priorities. Specifically, in conflict-prone areas, strategically reducing greenery, limiting architectural diversity in color and texture, and promoting greater spatial openness can effectively mitigate attentional distractions, thereby reducing perception–risk mismatches and enhancing cycling safety. Ultimately, this research advocates for an integrated human–vehicle–environment safety framework, calling for interdisciplinary collaboration between neuroscience, urban planning, and transport engineering to design urban spaces that minimize cycling accidents and improve overall road safety outcomes.

Reference

Aldred, R., 2016. Cycling near misses: Their frequency, impact, and prevention. Transportation Research Part A: Policy and Practice 90, 69-83.

Arnau, S., Löffler, C., Rummel, J., Hagemann, D., Wascher, E., Schubert, A.L., 2020. Inter-trial alpha power indicates mind wandering. Psychophysiology 57 (6), e13581.

Asgarzadeh, M., Lusk, A., Koga, T., Hirate, K., 2012. Measuring oppressiveness of streetscapes. Landscape and Urban Planning 107 (1), 1-11.

Bacigalupo, F., Luck, S.J., 2022. Alpha-band eeg suppression as a neural marker of sustained attentional engagement to conditioned threat stimuli. Social Cognitive and Affective Neuroscience 17 (12), 1101-1117.

Bazilinskyy, P., Eisma, Y., Dodou, D., De Winter, J.C., 2020. Risk perception: A study using dashcam videos and participants from different world regions. Traffic injury prevention 21 (6), 347-353.

Bidgoli, M.A., Behmanesh, A., Khademi, N., Thansirichaisree, P., Zheng, Z., Tehrani, S.S.M., Mazloum, S., Kongsilp, S., 2025. Brain activity patterns reflecting security perceptions of female cyclists in virtual reality experiments. Scientific Reports 15 (1), 761.

Bjerke, T., Østdahl, T., Thrane, C., Strumse, E., 2006. Vegetation density of urban parks and perceived appropriateness for recreation. Urban Forestry & Urban Greening 5 (1), 35-44.

Bogacz, M., Hess, S., Calastri, C., Choudhury, C.F., Mushtaq, F., Awais, M., Nazemi, M., Van Eggermond, M.A., Erath, A., 2021. Modelling risk perception using a dynamic hybrid choice model and brain-imaging data: An application to virtual reality cycling. Transportation research part C: emerging technologies 133, 103435.

Braboszcz, C., Delorme, A., 2011. Lost in thoughts: Neural markers of low alertness during mind wandering. Neuroimage 54 (4), 3040-3047.

Campisi, T., Deluka-Tibljaš, A., Tesoriere, G., Canale, A., Rencelj, M., Šurdonja, S., 2020. Cycling traffic at turbo roundabouts: Some considerations related to cyclist mobility and safety. Transportation research procedia 45, 627-634.

Chatterjee, D., Gavas, R., Saha, S.K., 2023. Detection of mental stress using novel spatio-temporal distribution of brain activations. Biomedical Signal Processing and Control 82, 104526.

Cho, G., Rodríguez, D.A., Khattak, A.J., 2009. The role of the built environment in explaining relationships between perceived and actual pedestrian and bicyclist safety. Accident Analysis & Prevention 41 (4), 692-702.

Choi, Y., Kim, M., Chun, C., 2015. Measurement of occupants' stress based on electroencephalograms (eeg) in twelve combined environments. Building and Environment 88, 65-72.

Conrad, C., Newman, A., 2021. Measuring mind wandering during online lectures assessed with eeg. Frontiers in Human Neuroscience 15, 697532.

Da Silva, M.D., Gonçalves, Ó.F., Branco, D., Postma, M., 2022. Revisiting consciousness: Distinguishing between states of conscious focused attention and mind wandering with eeg. Consciousness and Cognition 101, 103332.

Dang, M., Jin, Y., Hang, P., Crosato, L., Sun, Y., Wei, C., 2024. Coupling intention and actions of vehicle–pedestrian interaction: A virtual reality experiment study. Accident Analysis & Prevention 203, 107639.

Darzian Rostami, A., Katthe, A., Sohrabi, A., Jahangiri, A., 2020. Predicting critical bicycle-vehicle conflicts at signalized intersections. Journal of advanced transportation 2020 (1), 8816616.

Diarra, M., Marchitto, M., Bressolle, M.-C., Baccino, T., Drai-Zerbib, V., 2023. A narrative review of the interconnection between pilot acute stress, startle, and surprise effects in the aviation context: Contribution of physiological measurements. Frontiers in neuroergonomics 4, 1059476.

Dill, J., Mcneil, N., 2013. Four types of cyclists? Examination of typology for better understanding of bicycling behavior and potential. Transportation Research Record 2387 (1), 129-138.

Doorley, R., Pakrashi, V., Byrne, E., Comerford, S., Ghosh, B., Groeger, J.A., 2015. Analysis of heart rate variability amongst cyclists under perceived variations of risk exposure. Transportation research part F: traffic psychology and behaviour 28, 40-54.

Ewing, R., Handy, S., 2009. Measuring the unmeasurable: Urban design qualities related to walkability. Journal of Urban design 14 (1), 65-84.

Friedman, J.H., Popescu, B.E., 2008. Predictive learning via rule ensembles.

Galpin, A., Underwood, G., Crundall, D., 2009. Change blindness in driving scenes. Transportation research part F: traffic psychology and behaviour 12 (2), 179-185.

Ge, H., Xia, R., Sun, H., Yang, Y., Huang, M., 2019. Construction and simulation of rear-end conflicts recognition model based on improved ttc algorithm. IEEE Access 7, 134763-134771.

Griffin, W., Haworth, N., Twisk, D., 2020. Patterns in perceived crash risk among male and female drivers with and without substantial cycling experience. Transportation research part F: traffic psychology and behaviour 69, 1-12.

Guan, F., Fang, Z., Wang, L., Zhang, X., Zhong, H., Huang, H., 2022. Modelling people's perceived scene complexity of real-world environments using street-view panoramas and open geodata. ISPRS Journal of Photogrammetry and Remote Sensing 186, 315-331.

He, C., Xu, P., Pei, X., Wang, Q., Yue, Y., Han, C., 2024. Fatigue at the wheel: A non-visual approach to truck driver fatigue detection by multi-feature fusion. Accident Analysis & Prevention 199, 107511.

He, X., He, S.Y., 2023. Using open data and deep learning to explore walkability in shenzhen, china.

Transportation research part D: transport and environment 118, 103696.

He, Y., Sun, C., Huang, H., Jiang, L., Ma, M., Wang, P., Wu, C., 2021. Safety of micro-mobility: Riders' psychological factors and risky behaviors of cargo ttws in china. Transportation research part F: traffic psychology and behaviour 80, 189-202.

Heimstra, N.W., 1970. The effects of 'stress fatigue'on performance in a simulated driving situation. Ergonomics 13 (2), 209-218.

Htc Corporation, 2025. Vive pro 2 overview.

Ito, K., Biljecki, F., 2021. Assessing bikeability with street view imagery and computer vision. Transportation research part C: emerging technologies 132, 103371.

Jiang, B., Chang, C.-Y., Sullivan, W.C., 2014. A dose of nature: Tree cover, stress reduction, and gender differences. Landscape and urban planning 132, 26-36.

Jiang, B., He, J., Chen, J., Larsen, L., Wang, H., 2021. Perceived green at speed: A simulated driving experiment raises new questions for attention restoration theory and stress reduction theory. Environment and Behavior 53 (3), 296-335.

Jiang, B., Larsen, L., Deal, B., Sullivan, W.C., 2015. A dose–response curve describing the relationship between tree cover density and landscape preference. Landscape and urban planning 139, 16-25.

Jiang, B., Mak, C.N.S., Larsen, L., Zhong, H., 2017. Minimizing the gender difference in perceived safety: Comparing the effects of urban back alley interventions. Journal of Environmental Psychology 51, 117-131.

Johnson, M., Charlton, J., Oxley, J., Newstead, S., Year. Naturalistic cycling study: Identifying risk factors for on-road commuter cyclists. In: Proceedings of the Annals of advances in automotive medicine/annual scientific conference, pp. 275.

Kar, S., Bhagat, M., Routray, A., 2010. Eeg signal analysis for the assessment and quantification of driver's fatigue. Transportation research part F: traffic psychology and behaviour 13 (5), 297-306.

Kawshalya, L., Weerasinghe, U., Chandrasekara, D., 2022. The impact of visual complexity on perceived safety and comfort of the users: A study on urban streetscape of sri lanka. Plos one 17 (8), e0272074.

Kim, J.-H., Kim, D.-W., Im, C.-H., 2017. Brain areas responsible for vigilance: An eeg source imaging study. Brain topography 30 (3), 343-351.

Kononov, J., Allery, B., Znamenacek, Z., 2007. Safety planning study of urban freeways: Proposed methodology and review of case history. Transportation research record 2019 (1), 146-155.

Kovaceva, J., Nero, G., Bärgman, J., Dozza, M., 2019. Drivers overtaking cyclists in the real-world: Evidence from a naturalistic driving study. Safety science 119, 199-206.

Kwon, J.-H., Won, J., Cho, G.-H., 2024. Investigating the dynamics of collective behavior among pedestrians crossing roads: A multi-user virtual reality approach. Accident Analysis & Prevention 199, 107477.

Li, X., Yang, L., Yan, X., 2022. An exploratory study of drivers' eeg response during emergent collision avoidance. Journal of safety research 82, 241-250.

Llorca, C., Angel-Domenech, A., Agustin-Gomez, F., Garcia, A., 2017. Motor vehicles overtaking cyclists on two-lane rural roads: Analysis on speed and lateral clearance. Safety science 92, 302-310.

Luo, J., Liu, P., Xu, W., Zhao, T., Biljecki, F., 2025. A perception-powered urban digital twin to support human-centered urban planning and sustainable city development. Cities 156, 105473.

Luo, S., Xu, L., Tao, S., Fu, X., 2026. Non-linear impact of built environment on metro-bike integration from an eye-level perspective: A deep learning approach with street view images. Journal of Transport Geography 130, 104485.

Lynch, K., 1964. The image of the city MIT press.

Ma, L., Guo, Z., Lu, M., He, S., Wang, M., 2023. Developing an urban streetscape indexing based on visual complexity and self-organizing map. Building and Environment 242, 110549.

Ma, S., Yan, X., Billington, J., Merat, N., Markkula, G., 2024. Cognitive load during driving: Eeg microstate metrics are sensitive to task difficulty and predict safety outcomes. Accident Analysis & Prevention 207, 107769.

Magosso, E., De Crescenzio, F., Ricci, G., Piastra, S., Ursino, M., 2019. Eeg alpha power is modulated by attentional changes during cognitive tasks and virtual reality immersion. Computational intelligence and neuroscience 2019 (1), 7051079.

Manton, R., Rau, H., Fahy, F., Sheahan, J., Clifford, E., 2016. Using mental mapping to unpack perceived cycling risk. Accident Analysis & Prevention 88, 138-149.

Mekuria, M.C., Furth, P.G., Nixon, H., 2012. Low-stress bicycling and network connectivity.

Nazemi, M., Van Eggermond, M.A., Erath, A., Schaffner, D., Joos, M., Axhausen, K.W., 2021. Studying bicyclists' perceived level of safety using a bicycle simulator combined with immersive virtual reality. Accident Analysis & Prevention 151, 105943.

Olsson, S.R., Elldér, E., 2023. Are bicycle streets cyclist-friendly? Micro-environmental factors for improving perceived safety when cycling in mixed traffic. Accident Analysis & Prevention 184, 107007.

Palva, S., Palva, J.M., 2007. New vistas for α-frequency band oscillations. Trends in neurosciences 30 (4), 150-158.

Pucher, J., Buehler, R., 2008. Making cycling irresistible: Lessons from the netherlands, denmark and germany. Transport reviews 28 (4), 495-528.

Ramadhan, S.A., Joelianto, E., Sutarto, H.Y., 2019. Simulation of traffic control using vissim-com interface. Internetworking Indonesia Journal 11 (1), 55-61.

Rasch, A., Boda, C.-N., Thalya, P., Aderum, T., Knauss, A., Dozza, M., 2020. How do oncoming traffic and cyclist lane position influence cyclist overtaking by drivers? Accident Analysis & Prevention 142, 105569.

Rasch, A., Dozza, M., 2020. Modeling drivers' strategy when overtaking cyclists in the presence of oncoming traffic. IEEE transactions on intelligent transportation systems 23 (3), 2180-2189.

Rasch, A., Moll, S., López, G., Garcia, A., Dozza, M., 2022. Drivers' and cyclists' safety perceptions in overtaking maneuvers. Transportation research part F: traffic psychology and behaviour 84, 165-176.

Roth, S., Cohen, L.J., 1986. Approach, avoidance, and coping with stress. American psychologist 41 (7), 813.

Roxburgh, A.D., White, D.J., Grillon, C., Cornwell, B.R., 2023. A neural oscillatory signature of sustained anxiety. Cognitive, Affective, & Behavioral Neuroscience 23 (6), 1534-1544.

Sarkar, C., Webster, C., Pryor, M., Tang, D., Melbourne, S., Zhang, X., Jianzheng, L., 2015. Exploring associations between urban green, street design and walking: Results from the greater london boroughs. Landscape and Urban Planning 143, 112-125.

Schneider, R.J., Ryznar, R.M., Khattak, A.J., 2004. An accident waiting to happen: A spatial approach to proactive pedestrian planning. Accident Analysis & Prevention 36 (2), 193-211.

Seeber, M., Scherer, R., Wagner, J., Solis-Escalante, T., Müller-Putz, G.R., 2015. High and low gamma eeg oscillations in central sensorimotor areas are conversely modulated during the human gait cycle. Neuroimage 112, 318-326.

Simor, P., Vékony, T., Farkas, B.C., Szalárdy, O., Bogdány, T., Brezóczki, B., Csifcsák, G., Németh, D., 2025. Mind wandering during implicit learning is associated with increased periodic eeg activity and improved extraction of hidden probabilistic patterns. Journal of Neuroscience 45 (19).

Suzhou Planning Bureau, 2022. Suzhou annual transport report. Suzhou: Suzhou Planning Bureau.

Teh, E., Jamson, S., Carsten, O., Jamson, H., 2014. Temporal fluctuations in driving demand: The effect of traffic complexity on subjective measures of workload and driving performance. Transportation research part F: traffic psychology and behaviour 22, 207-217.

Teigen, K.H., 1995. How good is good luck? The role of counterfactual thinking in the perception of lucky and unlucky events. European Journal of Social Psychology 25 (3), 281-302.

Teigen, K.H., 1997. Luck, envy and gratitude: It could have been different. Scandinavian Journal of Psychology 38 (4), 313-323.

Teigen, K.H., 2005. The proximity heuristic in judgments of accident probabilities. British Journal of Psychology 96 (4), 423-440.

Teigen, K.H., Jensen, T.K., 2010. Unlucky victims or lucky survivors? European Psychologist.

Terum, J.A., Svartdal, F., 2019. Lessons learned from accident and near-accident experiences in traffic. Safety science 120, 672-678.

The State Council of the People's Republic of China, 2019. Regulations on the implementation of the road traffic safety law of the people's republic of china. The State Council of the People's Republic of China.

Ullmann, D., Kreimeier, J., Kipke, H., 2022. Pedaling through a virtually redesigned city: Evaluation of traffic planning and urban design factors influencing bicycle traffic. Journal of urban mobility 2, 100032.

Ulrich, R.S., Simons, R.F., Losito, B.D., Fiorito, E., Miles, M.A., Zelson, M., 1991. Stress recovery during exposure to natural and urban environments. Journal of environmental psychology 11 (3), 201-230.

Van Son, D., De Blasio, F.M., Fogarty, J.S., Angelidis, A., Barry, R.J., Putman, P., 2019. Frontal eeg theta/beta ratio during mind wandering episodes. Biological psychology 140, 19-27.

Wascher, E., Rasch, B., Sänger, J., Hoffmann, S., Schneider, D., Rinkenauer, G., Heuer, H., Gutberlet, I., 2014. Frontal theta activity reflects distinct aspects of mental fatigue. Biological psychology 96, 57-65.

Wei, C.-S., Wang, Y.-T., Lin, C.-T., Jung, T.-P., 2018. Toward drowsiness detection using non-hair-bearing eeg-based brain-computer interfaces. IEEE transactions on neural systems and rehabilitation engineering 26 (2), 400-406.

Wiedemann, R., Reiter, U., 1992. Microscopic traffic simulation: The simulation system mission, background and actual state. Project ICARUS (V1052) Final Report 2, 1-53.

Wilde, G.J., 1998. Risk homeostasis theory: An overview. Injury prevention 4 (2), 89-91.

Xu, L., Luo, S., Delbosc, A., O'hern, S., Chen, Z., 2026. Non-linear effects of built environment on cyclists' perceived safety and comfort using online pairwise voting. Transportation Research Part A: Policy and Practice 205, 104850.

Xu, L., Luo, S., O'hern, S., Delbosc, A., Chen, Z., Fu, X., 2025. Do protected cycle lanes make cities more bike-friendly? Integrating street view images with deep learning techniques. Cities 161, 105890.

Xu, Z., Zheng, N., Logan, D.B., Vu, H.L., 2023. Assessing bicycle-vehicle conflicts at urban intersections utilizing a vr integrated simulation approach. Accident Analysis & Prevention 191, 107194.

Yamada, F., 1998. Frontal midline theta rhythm and eyeblinking activity during a vdt task and a video game: Useful tools for psychophysiology in ergonomics. Ergonomics 41 (5), 678-688.

Yang, L., Zhou, R., Li, G., Yang, Y., Zhao, Q., 2025. Recognizing and explaining driving stress using a shapley additive explanation model by fusing eeg and behavior signals. Accident Analysis &

Prevention 209, 107835.

Ye, Y., Zhong, C., Suel, E., 2024. Unpacking the perceived cycling safety of road environment using street view imagery and cycle accident data. Accident Analysis & Prevention 205, 107677.

Yeom, S., Kim, H., Hong, T., 2021. Psychological and physiological effects of a green wall on occupants: A cross-over study in virtual reality. Building and Environment 204, 108134.

Zeuwts, L.H., Vansteenkiste, P., Deconinck, F.J., Cardon, G., Lenoir, M., 2017. Hazard perception in young cyclists and adult cyclists. Accident Analysis & Prevention 105, 64-71.

Zhang, S., Abdel-Aty, M., Cai, Q., Li, P., Ugan, J., 2020. Prediction of pedestrian-vehicle conflicts at signalized intersections based on long short-term memory neural network. Accident Analysis & Prevention 148, 105799.

Zhang, X., Yan, X., 2023. Predicting collision cases at unsignalized intersections using eeg metrics and driving simulator platform. Accident Analysis & Prevention 180, 106910.

Zhao, Y., Miyahara, T., Mizuno, K., Ito, D., Han, Y., 2021. Analysis of car driver responses to avoid car-to-cyclist perpendicular collisions based on drive recorder data and driving simulator experiments. Accident Analysis & Prevention 150, 105862.

Zhou, B., Zhao, H., Puig, X., Xiao, T., Fidler, S., Barriuso, A., Torralba, A., 2019. Semantic understanding of scenes through the ade20k dataset. International Journal of Computer Vision 127, 302-321.

Zhu, M., Sze, N., Newnam, S., 2022. Effect of urban street trees on pedestrian safety: A micro-level pedestrian casualty model using multivariate bayesian spatial approach. Accident Analysis & Prevention 176, 106818.